Inorganic Chemistry
Cite This: Inorg. Chem. XXXX, XXX, XXX−XXX
Article
pubs.acs.org/IC

Influence of Pyridine on the Multielectron Redox Cycle of Nickel Diethyldithiocarbamate

Chase S. Richburg and Byron H. Farnum*

Department of Chemistry and Biochemistry, Auburn University, Auburn, Alabama 36849, United States

Supporting Information

ABSTRACT: Two-electron (2e$^-$)-transfer reactions for monometallic complexes of first-row transition metals are uncommon because of the tendency of these metals to proceed through sequential one-electron (1e$^-$)-transfer pathways. For this chemistry to be observed, structural changes upon electron transfer are often needed to shift the 1e$^-$ redox potentials to a condition of potential inversion where 2e$^-$ transfer becomes favorable. Nickel(II) dithiocarbamate complexes take advantage of these conditions to drive 2e$^-$ oxidation from Ni^{II} to Ni^{IV}. Here, we have studied the electrochemistry of $Ni^{II}(dtc)_2$, where dtc$^-$ is *N,N*-diethyldithiocarbamate in an acetonitrile solvent as a function of the scan rate and added pyridine to gain further insight into the mechanism for its 2e$^-$ oxidation to $[Ni^{IV}(dtc)_3]^+$. The scan rate dependence revealed evidence for an ECE mechanism in which the chemical step constituted ligand exchange between $[Ni^{III}(dtc)_2]^+$ and $Ni^{II}(dtc)_2$. A pseudo-first-order rate constant for this reaction of 34 s^{-1} was obtained at 1 mM $Ni^{II}(dtc)_2$. The addition of pyridine to the electrolyte solution showed pronounced changes to the cyclic voltammetry (CV) that were consistent with the formation of a pyridine-bound Ni^{III} complex, $[Ni^{III}(dtc)_2(py)_2]^+$, which was stable at high scan rates but decomposed to $[Ni^{IV}(dtc)_3]^+$ at low scan rates. The observed decomposition rate constant was well modeled with two parallel decay pathways, one through the dipyridine $[Ni^{III}(dtc)_2(py)_2]^+$ and another through a monopyridine $[Ni^{III}(dtc)_2py]^+$. Overall, these data point to a mechanism for oxidation from $Ni^{II}(dtc)_2$ to $[Ni^{IV}(dtc)_3]^+$ that proceeds through an undercoordinated $[Ni^{III}(dtc)_2]^+$ complex, which can be trapped on the time scale of CV experiments using pyridine ligands. These studies provide insight into how we may be able to control 1e$^-$ versus 2e$^-$ redox chemistry using the coordination environment and nickel oxidation state.

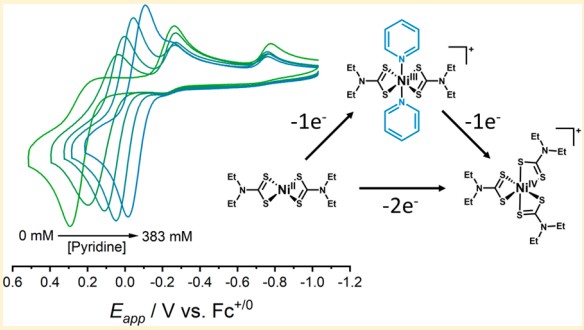

INTRODUCTION

Electron-transfer reactions with first-row transition metals typically follow one-electron (1e$^-$) pathways. Therefore, many synthetic first-row metal complexes that have shown multielectron reactivity incorporate multiple metal centers, where each is oxidized/reduced by 1e$^-$.[1−16] For complexes that achieve multielectron redox chemistry at monometallic centers, however, structural changes around the metal center and/or noninnocent ligands have been utilized to force a multielectron pathway over single electron transfer.[17−28] In these examples, the 1e$^-$ redox potentials associated with the metal center are shifted from their normal ordering to a condition known as potential inversion.[29]

Figure 1 illustrates the concept of structure-induced potential inversion. Here, $E_{1A}°$ and $E_{2A}°$ are 1e$^-$ redox potentials associated with changes in the oxidation state of a metal center, where the coordination environment (A) is unchanged between oxidation states. These could be imagined as the $M^{IV/III}$ ($E_{1A}°$) and $M^{III/II}$ ($E_{2A}°$) reduction potentials in their normal ordering; i.e., a more cathodic potential is required to reduce $M^{III} \rightarrow M^{II}$ than $M^{IV} \rightarrow M^{III}$. A change in the structure to a new coordination environment (B) produces two new reduction potentials at $E_{1B}°$ and $E_{2B}°$ for the same changes in the oxidation state. The differences in environments A and B could be due to changes in the coordination number, isomerization, or both. The differences in energy $E_{1A}° - E_{1B}°$ and $E_{2A}° - E_{2B}°$ represent the difference in free energy between the oxidized and reduced states in each coordination environment, ΔG_{1AB} and ΔG_{2AB}, respectively. A large difference indicates that environment B is greatly preferred by the higher oxidation state over the lower oxidation state. Likewise, environment A is highly favored by the lower oxidation state compared with the higher oxidation state. Potential inversion therefore arises in this system if the most oxidized state M^{IV} strongly prefers environment B and the most reduced state M^{II} strongly prefers environment A. Under these conditions, a two-electron (2e$^-$) redox potential then emerges at $E_{2e^-}° = (E_{2A}° - E_{1B}°)/2$. Importantly, the mechanism of the 2e$^-$ redox event occurs through a rapid sequence of 1e$^-$ $M^{III/II}$ and $M^{IV/III}$ redox reactions, where the M^{III} oxidation state is an unstable intermediate.

Examples of such structural changes known to induce potential inversion include ligand coordination, ligand

Received: August 10, 2019

DOI: 10.1021/acs.inorgchem.9b02430
Inorg. Chem. XXXX, XXX, XXX−XXX

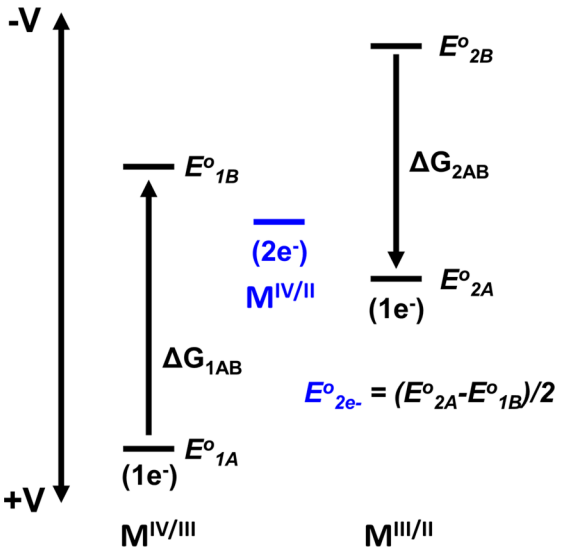

Figure 1. Electrochemical energy diagram showing how structural changes between coordination environments (A and B) can induce potential inversion of the 1e$^-$ redox potentials. In the hypothetical redox cycle, the M^{IV} oxidation state prefers environment B and the M^{II} oxidation state prefers environment A, thus forcing the $M^{IV/III}$ potential ($E_{1B}°$) more cathodic than the $M^{III/II}$ potential ($E_{2A}°$). A 2e$^-$ redox potential will thus be favored at $E_{2e^-}° = (E_{2A}° - E_{1B}°)/2$.

dissociation, and changes in the ligand hapticity.[17,20−23,26−28] For example, 2e$^-$ reduction of $[Ni^{II}(bpy)_3]^{2+}$, where bpy is 2,2′-bipyridine, results in the formation of $Ni^0(bpy)_2$ and loss of a bpy ligand.[22] Likewise, the reduction of some manganese and ruthenium arene complexes has shown a decrease in the hapticity from η^6 to η^4 upon 2e$^-$ reduction.[17,27,28] In general, increases in the coordination number around the metal center lead to more cathodic reduction potentials (i.e., environment B), while decreases lead to more anodic potentials (i.e., environment A). The energy required for the structural change to induce potential inversion is typically large, and therefore simple ligand coordination/dissociation without reorganization of the coordination environment often does not result in 2e$^-$ behavior. For example, axial ligand coordination/dissociation to metal centers in tetraazamacrocycles does not typically result in 2e$^-$ redox chemistry; however, there are some noted cases.[30,31]

One class of molecules that is interesting in this context is nickel dithiocarbamates ($Ni^{II}(dtc)_2$), which are known to undergo 2e$^-$ oxidation from Ni^{II} to Ni^{IV}.[20,21,32] This reaction takes advantage of structural changes around the metal center to influence the 1e$^-$ $Ni^{IV/III}$ and $Ni^{III/II}$ reduction potentials to achieve potential inversion. Specifically, the oxidation process converts a square-planar $Ni^{II}(dtc)_2$ molecule into octahedral $[Ni^{IV}(dtc)_3]^+$. Reorganization of the dithiocarbamate ligand framework from a square-planar environment to cis-octahedral coupled with the coordination of a third dtc$^-$ ligand imparts a significant amount of reorganization to the system that influences the 1e$^-$ reduction potentials. The structures of both oxidation states for a number of dithiocarbamate ligands have been characterized, with their general structures shown in Figure 2.[33−38] The assignment of the Ni^{IV} oxidation state is unique from the perspective of other highly oxidized nickel−sulfur complexes such as nickel dithiolenes where the 1,2-dithio functionality of the ligand results in ligand-based oxidation instead of the metal.[39−42] When coordinated to

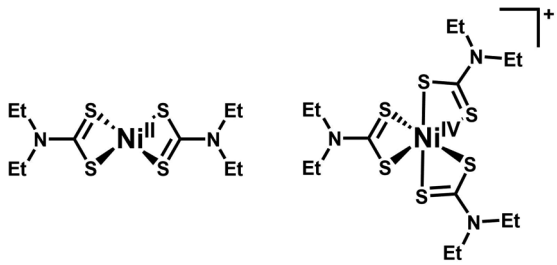

Figure 2. Chemical structures of $Ni^{II}(dtc)_2$ and $[Ni^{IV}(dtc)_3]^+$, where dtc$^-$ is *N*,*N*-diethyldithiocarbamate.

nickel, the 1,1-dithio functionality of the dithiocarbamates is more difficult to oxidize than the metal, and therefore metal-based oxidation is observed.

Although 2e$^-$ oxidation is highly favored, reduction of Ni^{IV} back to Ni^{II} occurs through a different pathway involving two sequential 1e$^-$ reductions (i.e., $[Ni^{IV}(dtc)_3]^+ \rightarrow Ni^{III}(dtc)_3 \rightarrow Ni^{II}(dtc)_2$) because of the strongly chelated cis-octahedral environment. Previous studies have reported the electrochemistry of $Ni^{II}(dtc)_2$ molecules but have not investigated the mechanistic details for conversion between Ni^{II} and Ni^{IV} oxidation states. All 2e$^-$-transfer reactions must proceed through 1e$^-$ intermediates, even if the intermediates are extremely short-lived and conversion to the 2e$^-$ product is rapid.[29] This means that details surrounding the Ni^{III} oxidation state are greatly important in understanding the kinetic and thermodynamic factors that dictate 2e$^-$ versus 1e$^-$ redox chemistry. Research efforts to better understand what factors influence this complicated redox cycle could lead to the development of reversible 2e$^-$ couples based on nickel dithiocarbamates. It is also notable that the ability of nickel-based catalysts to proceed through 2e$^-$ versus 1e$^-$ pathways has become an area of great interest.[43−52]

Lachenal proposed that favorable 2e$^-$ oxidation from Ni^{II} to Ni^{IV} is due to the formation of an unstable $[Ni^{III}(dtc)_2]^+$ intermediate following 1e$^-$ oxidation of $Ni^{II}(dtc)_2$; however, no evidence for this species has been presented. The unsaturated coordination environment of this intermediate may therefore be susceptible to influence by the addition of ancillary ligands such as pyridine, which would allow for competitive mechanistic studies to be performed. Here we present an electrochemical study on the influence of pyridine on the multielectron redox cycle of a $Ni^{II}(dtc)_2$ complex, where dtc$^-$ is *N*,*N*-diethyldithiocarbamate. The scan rate dependence of $Ni^{II}(dtc)_2$ with and without added pyridine uncovers new information about the mechanism of 2e$^-$ transfer and the importance of reactions related to transferring dithiocarbamate ligands to oxidized nickel centers. Specifically, the addition of pyridine shows the ability to trap intermediate Ni^{III} oxidation states prior to ligand exchange and subsequent oxidation to Ni^{IV}.

■ EXPERIMENTAL SECTION

Synthesis and Characterization of $Ni^{II}(dtc)_2$. Nickel(II) diethyldithiocarbamate $[Ni^{II}(dtc)_2]$ was prepared as previously described.[20] A total of 2 equiv of sodium diethyldithiocarbamate trihydrate (Sigma, >99.0%) was added to 1 equiv of nickel(II) chloride hexahydrate (Alfa Aesar, 98%) dissolved in distilled water. A green solid precipitated immediately and was filtered under vacuum and washed with cold distilled water, ethanol, and ether with 96% yield. Characterization of the light-green solid was performed by ^{1}H

DOI: 10.1021/acs.inorgchem.9b02430
Inorg. Chem. XXXX, XXX, XXX−XXX

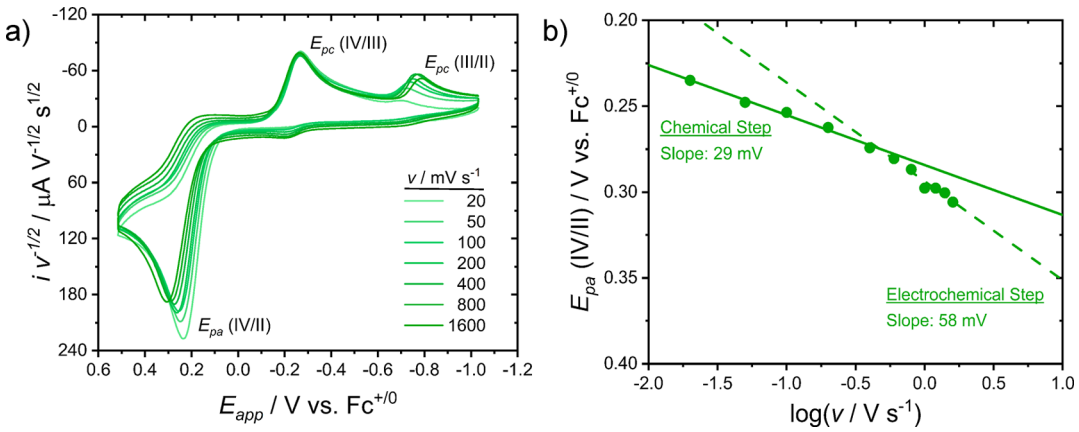

Figure 3. (a) CV data for 1 mM $Ni^{II}(dtc)_2$ in MeCN (0.1 M $TBAPF_6$) at room temperature. The current is shown normalized to the scan rate (v) by dividing by $v^{1/2}$. Shifts in the peak currents and peak potentials indicate the presence of redox reactions coupled to chemical steps in a homogeneous solution. (b) E_{pa}(IV/II) plotted versus log(v).

NMR (acetonitrile-d_3): δ 3.57 (q, $-CH_2-$), 1.17 (t, $-CH_3$) and UV−vis spectroscopy [λ_{max}, nm (ε, M^{-1} cm^{-1})]: 388 (5600), 323 (26700).

Electrochemistry. Tetrabutylammonium hexafluorophosphate ($TBAPF_6$; Sigma-Aldrich, 98%) was recrystallized in absolute ethanol, then dried under vacuum, and stored in a desiccator. All cyclic voltammetry (CV) experiments were performed with 0.1 M $TBAPF_6$ and acetonitrile (MeCN; VWR Chemicals, HPLC grade) electrolytes in a nitrogen-purged environment. Experiments were performed at room temperature using a WaveDriver 20 bipotentiostat (Pine Research) with a glassy-carbon-disk working electrode (Pine Research, 5 mm diameter), a Ag/Ag^+ nonaqueous reference electrode (BASi Instruments) with 0.001 M $AgNO_3$ in MeCN, and a platinum-wire counter electrode. The glassy carbon working electrode was polished with 0.05 μm alumina powder (Allied High Tech Products Inc., DeAgglomerated). The reduction potential of ferrocene (Fc; Alfa Aesar, 99%) was recorded before and after all electrochemical experiments to confirm the consistency in the reference electrode. All potentials are reported versus the $Fc^{+/0}$ couple. All experiments were collected after compensating for the internal solution resistance and consisted of three continuous cycles starting at E_{app} = −1.02 V and scanned with an initial positive direction over the potential range. Data shown are those of the third cycle. Pyridine (Sigma-Aldrich, anhydrous, 99.8%) titrations were performed directly from a sample of pure pyridine (12 M) purged with nitrogen.

Spectroelectrochemistry. Spectroelectrochemical experiments were performed with a WaveDriver 20 bipotentiostat using 0.1 M lithium bis(trifluoromethane)sulfonimide (Sigma, 99.95%) in MeCN as the electrolyte. In this experimental setup, both the working and counter electrodes were present on a platinum honeycomb electrode (Pine Research), and the reference electrode was a low-profile Ag/Ag^+ nonaqueous electrode (Pine Research). [$Ni^{II}(dtc)_2$] in all electrochemical experiments was 1.0 mM. UV−vis absorbance spectra were collected simultaneously using an AvaAspec-2048 fiber-optic spectrometer (Avantes) and a thin-path-length (2 mm) cuvette. Spectra were recorded for each applied potential after being held for a period of 30 s to ensure the establishment of redox equilibrium.

Electrochemical Modeling. *DigiElch*, version 8, was used to model the CV data and generate a working curve for analysis of the rate constants in the presence of pyridine. The Supporting Information provides detailed information regarding the methods and parameters.

Electron Paramagnetic Resonance (EPR). EPR samples were prepared by dissolving $Ni^{II}(dtc)_2$, pyridine, and acetylferrocenium ($AcFc^+$) in the proper ratio in a MeCN solvent and quickly transferring to an EPR tube, where the sample was frozen using liquid nitrogen. $AcFc^+$ was synthesized according to previous reports.[53] Continuous-wave EPR spectra were measured at the X-band (9 GHz) frequency on a Bruker EMX spectrometer fitted with an ER-4119-HS (high-sensitivity) perpendicular-mode cavity. All measurements were collected at 77 K and performed by fitting the cavity with a liquid-nitrogen finger dewar. Spectra were recorded with a field modulation frequency of 100 kHz, a modulation amplitude of 6.00 G, a microwave power of 1.995 mW, and a frequency of 9.370 GHz.

RESULTS

Electrochemistry. CV experiments performed with $Ni^{II}(dtc)_2$ in MeCN solvents were qualitatively consistent with those previously reported by Martin in acetone and Lachenal in MeCN.[20,21] Figure 3a shows the CV data for 1 mM $Ni^{II}(dtc)_2$ as a function of the scan rate (v) with the current normalized to $v^{1/2}$, with peak potentials and peak currents reported in Tables S1−S7. At v = 100 mV s^{-1}, an irreversible oxidation is observed at E_{pa}(IV/II) = 0.27 V assigned to the oxidation of four-coordinate $Ni^{II}(dtc)_2$ to six-coordinate $[Ni^{IV}(dtc)_3]^+$ via eq 1. The stoichiometry of this process is complex because of the ligand-exchange reaction that must occur in order to yield $[Ni^{IV}(dtc)_3]^+$. The consumption of a secondary $Ni^{II}(dtc)_2$ molecule results in an overall number of electrons transferred per $Ni^{II}(dtc)_2$ of n = $^4/_3$, despite Ni^{II} being oxidized by $2e^-$ to Ni^{IV}. Controlled potential electrolysis experiments have confirmed this stoichiometry.[21] Subsequent reduction of $[Ni^{IV}(dtc)_3]^+$ to $Ni^{II}(dtc)_2$ occurs through two irreversible reductions at E_{pc}(IV/III) = −0.27 and E_{pc}(III/II) = −0.74 V via eqs 2 and 3, respectively. Although all three redox waves are electrochemically irreversible, the entire cycle is reproducible and always regenerates $Ni^{II}(dtc)_2$ upon returning to cathodic potentials.

$$3Ni^{II}(dtc)_2 \rightleftharpoons 2[Ni^{IV}(dtc)_3]^+ + Ni^{II} + 4e^- \quad (1)$$

$$2\{[Ni^{IV}(dtc)_3]^+ + e^- \rightleftharpoons Ni^{III}(dtc)_3\} \quad (2)$$

$$2Ni^{III}(dtc)_3 + Ni^{II} + 2e^- \rightleftharpoons 3Ni^{II}(dtc)_2 \quad (3)$$

The scan rate dependence of $Ni^{II}(dtc)_2$ oxidation demonstrates that E_{pa}(IV/II) shifts positive with increasing scan rates. Great care was taken to correct for internal solution resistance to ensure the accuracy of the peak potentials. Figure 3b exhibits that, at low scan rates, E_{pa}(IV/II) versus log(v) shows a linear dependence with a slope of 29 mV dec^{-1}, while at high scan rates, the data are linear with a slope of 58 mV dec^{-1}. This behavior is consistent with an ECE/DISP mechanism for the oxidation of Ni^{II} to Ni^{IV} described by eqs 4−7.[21,54−56] Here, E

DOI: 10.1021/acs.inorgchem.9b02430
Inorg. Chem. XXXX, XXX, XXX−XXX

stands for an electrochemical step at the electrode surface, C stands for a chemical reaction step in a homogeneous solution, and DISP refers to an inherent disproportionation reaction that is competitive with the second electrochemical step. Within this mechanistic framework, electrochemical oxidation from $Ni^{II}(dtc)_2$ to $[Ni^{III}(dtc)_2]^+$ occurs first (eq 4), followed by ligand exchange with a second $Ni^{II}(dtc)_2$ to produce $Ni^{III}(dtc)_3$ (eq 5). Finally, $Ni^{III}(dtc)_3$ may be either oxidized by the electrode via the second E step (eq 6) or disproportionate with $[Ni^{III}(dtc)_2]^+$ (eq 7). Because of the fact that the chemical step consumes a second $Ni^{II}(dtc)_2$ molecule, this mechanism is specifically referred to as a radical substrate dimerization (RSD-ECE/DISP) and is often observed for the electrochemistry of halides, sulfides, organic radicals, and some organometallic species.[54,56−58]

$$\text{E} \qquad Ni^{II}(dtc)_2 \rightleftharpoons [Ni^{III}(dtc)_2]^+ + e^- \tag{4}$$

$$\text{C} \qquad 2[Ni^{III}(dtc)_2]^+ + Ni^{II}(dtc)_2 \rightleftharpoons 2Ni^{III}(dtc)_3 + Ni^{II} \tag{5}$$

$$\text{E} \qquad Ni^{III}(dtc)_3 \rightleftharpoons [Ni^{IV}(dtc)_3]^+ + e^- \tag{6}$$

$$\text{DISP} \qquad [Ni^{III}(dtc)_2]^+ + Ni^{III}(dtc)_3 \rightleftharpoons Ni^{II}(dtc)_2 + [Ni^{IV}(dtc)_3]^+ \tag{7}$$

The slope of 58 mV dec^{-1} at high scan rates indicates that $E_{pa}(IV/II)$ is controlled by the quasi-reversible electron-transfer kinetics associated with the oxidation of $Ni^{II}(dtc)_2$ to $[Ni^{III}(dtc)_2]^+$. The slope of 29 mV dec^{-1} at low scan rates indicates that the kinetics describing the ligand-exchange reaction are exhibiting chemical control over the magnitude of $E_{pa}(IV/II)$. In this regime, the scan rate is slow enough to allow for the chemical step to proceed appreciably and thus control the concentration of $[Ni^{III}(dtc)_2]^+$ at the electrode surface. The second electron-transfer step needed to oxidize $Ni^{III}(dtc)_3$ to $[Ni^{IV}(dtc)_3]^+$ or the disproportionation reaction has no bearing on $E_{pa}(IV/II)$; however, they do influence the peak current, $i_{pa}(IV/II)$.[54,56] As shown in Figure S1, the scan-rate-normalized current, $i_{pa}(IV/II)v^{-1/2}$, increases for low scan rates because of the ability for the chemical step to sufficiently produce $Ni^{III}(dtc)_3$ and thus allow for further oxidation. At appreciably fast scan rates, the reduction of $[Ni^{III}(dtc)_2]^+$ at the electrode surface occurs faster than ligand exchange and the current stabilizes to a value consistent with $1e^-$ transfer.

The rate constants for eqs 4 and 5 can be extracted from the scan rate dependence of $E_{pa}(IV/II)$ using eqs 8 and 9, respectively.[54,56] Here, $E°$ is the standard reduction potential for the $[Ni^{III}(dtc)_2]^+/Ni^{II}(dtc)_2$ redox couple, R is the ideal gas constant, T is the temperature (298 K), F is Faraday's constant, n is the number of electrons transferred in eq 4 ($n = 1$), α is the electron-transfer exchange coefficient, and λ is the unitless kinetic parameter associated with each step. For a chemically controlled step, $\lambda_c = k_cRT/nFv$, where k_c is the apparent first-order rate constant (s^{-1}) for the chemical step. For an electrochemically controlled step, $\lambda_E = k_E{}^2RT/\alpha nFDv$, where k_E is the rate constant for electron transfer at the electrode surface (cm s^{-1}) and D is the diffusion coefficient (cm^2 s^{-1}) of the redox-active molecule. The standard reduction potential for the $[Ni^{III}(dtc)_2]^+/Ni^{II}(dtc)_2$ redox couple was estimated to be $E° = 0.25$ V based on data collected between 4000 and 40000 mV s^{-1} (Figure S2), where the reduction of $[Ni^{III}(dtc)_2]^+$ could be observed by outcompeting the chemical step. Extrapolation of the low-scan-rate data in Figure 3b to the condition of $\log(v) = 0$ allowed for $k_c = 34$ s^{-1} to be estimated. On the basis of the complex stoichiometry of the ligand-exchange reaction in eq 5, this observed first-order rate constant is likely the result of a rate-determining step such as a reaction between $[Ni^{III}(dtc)_2]^+$ and $Ni^{II}(dtc)_2$, which could be taken as a pseudo-first-order reaction with excess $Ni^{II}(dtc)_2$. Taking the general assumption that $D = 10^{-5}$ cm^2 s^{-1}, extrapolation of high-scan-rate data to $\log(v) = 0$ yielded an estimate of $\alpha = 0.51$ based on the slope of 58 mV dec^{-1} and $k_E = 0.018$ cm s^{-1} from the intercept.[54,56,59]

$$E_{pa}(IV/II) = E° + 1.15(RT/nF) - (RT/2nF)\ln\lambda_C \tag{8}$$

$$E_{pa}(IV/II) = E° + 1.15(RT/\alpha nF) - (RT/2\alpha nF)\ln\lambda_E \tag{9}$$

The reduction of $[Ni^{IV}(dtc)_3]^+$ to $Ni^{III}(dtc)_3$ by eq 2 showed very little dependence on the scan rate, indicating that the reduction occurs with a large electron-transfer rate constant. Figure S3 shows a plot of $E_{pc}(IV/III)$ versus $\log(v)$, where the cathodic peak remains between −0.26 and −0.27 V from 20 to 1600 mV s^{-1}. In contrast, the reduction of $Ni^{III}(dtc)_3$ to $Ni^{II}(dtc)_2$ via eq 3 exhibits an obvious dependence of $E_{pc}(III/II)$ on the scan rate (Figure S4). The slope of $E_{pc}(III/II)$ versus $\log(v)$ is 38 mV dec^{-1} and indicates an EC mechanism described by eqs 10 and 11. Here, $1e^-$ reduction of $Ni^{III}(dtc)_3$ to $[Ni^{II}(dtc)_3]^-$ occurs as the E step and ligand exchange with a Ni^{II} ion occurs as the C step. $E_{pc}(III/II)$ can be analyzed by eq 12, where λ_C has the same definition as above to determine an apparent rate constant of $k_c(III/II) = 1.0$ s^{-1} for the chemical step. Given the complexity of the reaction shown in eq 11, this observed rate constant is best viewed as that for a rate-determining step. We do not presently know the nature of this step but could envision $[Ni^{II}(dtc)_3]^-$ dissociation or reaction with a Ni^{II} ion as a possible pathway.

$$\text{E} \qquad Ni^{III}(dtc)_3 + e^- \rightleftharpoons [Ni^{II}(dtc)_3]^- \tag{10}$$

$$\text{C} \qquad 2[Ni^{II}(dtc)_3]^- + Ni^{II} \rightleftharpoons 3Ni^{II}(dtc)_2 \tag{11}$$

$$E_{pc}(III/II) = E° - 0.78(RT/nF) + (RT/2nF)\ln\lambda_C \tag{12}$$

The normalized peak current for $Ni^{III}(dtc)_3$ reduction $[i_{pc}(III/II)v^{-1/2}]$ was also observed to increase prominently with faster scan rates (Figure S1). We believe that this behavior is consistent with a preceding chemical step that controls the concentration of $Ni^{III}(dtc)_3$ prior to reduction by eq 3. We believe this step to be the reverse ligand-exchange reaction of eq 5, i.e., $2Ni^{III}(dtc)_3 + Ni^{II} \rightarrow 2[Ni^{III}(dtc)_2]^+ + Ni^{II}(dtc)_2$. The reduction of $[Ni^{III}(dtc)_2]^+$ by the electrode or disproportionation by eq 7 could then result in $Ni^{II}(dtc)_2$.

To test this hypothesis, excess dithiocarbamate ligands Na(dtc) were added to the electrolyte to coordinate free Ni^{II} ions produced during oxidation. Figure 4 shows voltammograms measured with 1 mM Na(dtc) and 1 mM $Ni^{II}(dtc)_2$ as a function of the scan rate. The reduction of $Ni^{III}(dtc)_3$ to $Ni^{II}(dtc)_2$ near −0.75 V exhibits a much larger scan-rate dependence in the presence of excess dtc^- than in its absence. Much like the data shown in Figure 3, $i_{pc}(III/II)$ increases with larger scan rates. However, in the presence of dtc^-, $i_{pc}(III/II)$ increases to values equal to that of $i_{pc}(IV/III)$. This indicates that $Ni^{III}(dtc)_3$ is further preserved in the presence of excess

DOI: 10.1021/acs.inorgchem.9b02430
Inorg. Chem. XXXX, XXX, XXX−XXX

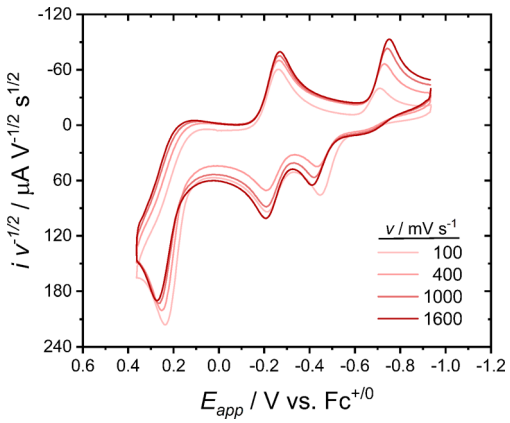

Figure 4. CV data for 1 mM $Ni^{II}(dtc)_2$ with 1 mM Na(dtc) in MeCN (0.1 M $TBAPF_6$) at room temperature.

dithiocarbamate ligands. We believe that this behavior is due to the coordination of excess dtc^- ligands with Ni^{II} ions, which lowers the concentration of Ni^{II} available for ligand exchange. Other notable features observed in the presence of excess dtc^- include the irreversible oxidation of dtc^- to $dtc^\bullet$ at $E_{pa} = -0.45$ V (100 mV s^{-1}) and an increase in the current associated with reversible oxidation from $Ni^{III}(dtc)_3$ to $[Ni^{IV}(dtc)_3]^+$ at $E_{pa} = -0.21$ V (100 mV s^{-1}). This behavior has been described previously as the chemical oxidation of $Ni^{II}(dtc)_2$ by $dtc^\bullet$ to produce $Ni^{III}(dtc)_3$, whereby $1e^-$ oxidation may proceed to $[Ni^{IV}(dtc)_3]^+$.[20] Interestingly, the peak potential and current for the oxidation of $Ni^{II}(dtc)_2$ to $[Ni^{IV}(dtc)_3]^+$ were not greatly affected by excess dtc^-. This is believed to be the result of dtc^- depletion at the electrode surface due to oxidation and consumption at more negative potentials, thus leaving no significant concentration available to coordinate to the oxidized nickel center.

Pyridine Addition. The ligand-exchange reaction shown in eq 5 is clearly an important step in both the oxidation of $Ni^{II}(dtc)_2$ and the reduction of $Ni^{III}(dtc)_3$. The details of this reaction are not currently well understood and likely involve multiple individual steps to achieve the overall reaction. We surmise that the solvent must play a role in stabilizing species such as $[Ni^{III}(dtc)_2]^+$, Ni^{II} ions, or possible intermediates such as bridged dimers capable of facilitating ligand exchange. Thus, CV experiments were conducted for $Ni^{II}(dtc)_2$ dissolved in MeCN with controlled additions of pyridine (py) to investigate the effect of a more strongly coordinating solvent ligand. Figure 5a shows CV data collected at 1000 mV s^{-1} for 1 mM $Ni^{II}(dtc)_2$ in MeCN over a range of [py] = 0−383 mM. The $Ni^{II}(dtc)_2$ oxidation peak was found to shift in a cathodic direction from +0.30 to −0.02 V over this concentration range, while the reversibility of the redox wave increased. The increase in the reversibility of this shifted redox feature was concomitant with a noticeable loss in the peak current associated with the reduction of $[Ni^{IV}(dtc)_3]^+$, i.e., i_{pc}(IV/III). This could also be observed in the scan-rate-dependent normalized voltammograms shown in Figures 5b and S5, where the rise of the new cathodic peak near −0.1 V at higher scan rates occurred with a decrease in the peak current for i_{pc}(IV/III).

The peak splitting of the shifted redox wave was found to be $\Delta E_p = E_{pa} - E_{pc} = 62$ mV at $v = 100$ mV s^{-1} and 91 mV at $v = 1000$ mV s^{-1}, consistent with a quasi-reversible $1e^-$-transfer reaction. This new redox wave is therefore proposed to be the result of $Ni^{II}(dtc)_2$ oxidation to a pyridine-coordinated $[Ni^{III}(dtc)_2(py)_x]^+$ complex (eq 13). EPR experiments confirmed the presence of Ni^{III} using $AcFc^+$ as a chemical oxidant (Figure S6). The observed signal was in the range of $g \sim 2.13$, consistent with other reports of $S = {}^1/_2$ Ni^{III} species; however, the signal changed significantly with increased pyridine concentration.[60,61] Further experiments are currently underway to decipher this behavior and characterize the pyridine-coordinated Ni^{III} structure. Notably, the EPR signal was only observed in the presence of oxidant and pyridine, with oxidant only conditions yielding and EPR-silent species believed to be low-spin $[Ni^{IV}(dtc)_3]^+$.[34]

$$Ni^{II}(dtc)_2 + x\text{py} \rightarrow [Ni^{III}(dtc)_2(\text{py})_x]^+ + e^- \quad (13)$$

$$[Ni^{III}(dtc)_2]^+ + x\text{py} \rightarrow [Ni^{III}(dtc)_2(\text{py})_x]^+ \quad (14)$$

$$E_{1/2} = E^o - (RT/F)\ln(K[\text{py}]^x) \quad (15)$$

Equation 13 likely proceeds by an EC mechanism where $Ni^{II}(dtc)_2$ is first oxidized to $[Ni^{III}(dtc)_2]^+$, followed by the addition of pyridine. This is reasoned based on the equilibrium constant for $Ni^{II}(dtc)_2(py)_2$ formation reported to be 0.087 M^{-2} and supported by ^1H NMR and UV−vis data collected here, which show little change in the $Ni^{II}(dtc)_2$ properties over the concentration range of pyridine studied (Figures S7 and

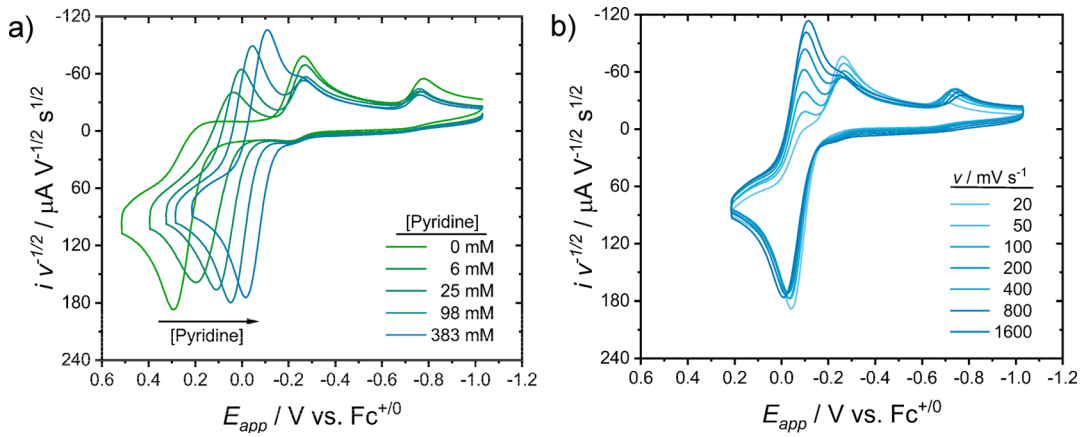

Figure 5. (a) CV data of 1 mM $Ni^{II}(dtc)_2$ in MeCN with added pyridine at $v = 1000$ mV s^{-1}. (b) CV data of 1 mM $Ni^{II}(dtc)_2$ and 383 mM pyridine in MeCN collected as a function of the scan rate. All data were collected with a 0.1 M $TBAPF_6$ electrolyte at room temperature.

DOI: 10.1021/acs.inorgchem.9b02430
Inorg. Chem. XXXX, XXX, XXX−XXX

S8).[62] Using this value, we calculate $[Ni^{II}(dtc)_2(py)_2]$ = 0.013 mM at the highest concentration of pyridine (383 mM), or 1.3% of the total $Ni^{II}(dtc)_2$ in solution. The equilibrium constant for pyridine coordination to $[Ni^{III}(dtc)_2]^+$ (eq 14) was determined using the shift in $E_{1/2}$ as a function of the pyridine concentration (Table 1) according to eq 15, where $E°$ = 0.25 V is the standard potential for the $[Ni^{III}(dtc)_2]^+/Ni^{II}(dtc)_2$ couple. A plot of $K[py]^x$ versus [py] is shown in Figure 6, where a clear second-order dependence on pyridine (x = 2) can be observed, indicating that $[Ni^{III}(dtc)_2(py)_2]^+$ is the ultimate product. The equilibrium constant for the coordination of two pyridine ligands was extracted with a quadratic fit to yield an average estimate of K = 1.4 (±0.2) × 10^6 M^{-2}, obtained using data collected over a range in the scan rates of 100−1600 mV s^{-1} (Table S8). On the basis of this equilibrium constant, $E_{1/2}$ = −0.24 V would be expected in a pure pyridine solvent ([py] = 12.4 M). Indeed, Figure S9 shows the CV data collected in pure pyridine, where $E_{1/2}$ = −0.28 V was experimentally measured, consistent with our calculated estimate.

Table 1. Summary of $E_{1/2}$ and k_{dec} Measured for the $Ni^{III}(dtc)_2(py)_2/Ni^{II}(dtc)_2$ Redox Couple as a Function of the Pyridine Concentration

[py]/mM	$E_{1/2}$/V vs $Fc^{+/0}$	k_{dec}/s^{-1}
0		
3	0.14	9.9
6	0.12	6.3
12	0.09	4.2
25	0.06	2.8
49	0.03	2.1
98	0.00	1.6
195	−0.03	1.0
383	−0.06	0.8

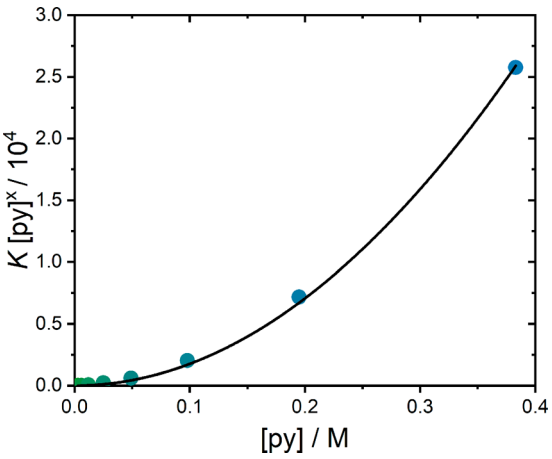

Figure 6. Determination of the equilibrium constant [K = 1.4 (±0.2) × 10^6 M^{-2}] for pyridine coordination to $[Ni^{III}(dtc)_2]^+$ based on eqs 14 and 15

The rate constant for pyridine coordination could not be measured using scan-rate-dependent techniques like those used to analyze the chemical step in the absence of pyridine, given the fact that the addition of pyridine results in a quasi-reversible redox feature. These methods are only valid when the chemically coupled electron-transfer reaction is in the so-called pure kinetic region that is achieved when the redox wave is completely irreversible.[54−56] Furthermore, the quasi-reversibility of the pyridine-coupled wave is actually related to the decomposition of $[Ni^{III}(dtc)_2(py)_2]^+$, not its formation. Evidence for this assignment is found in the inverse dependence of the cathodic peak currents between the $[Ni^{III}(dtc)_2(py)_2]^+/Ni^{II}(dtc)_2$ and $[Ni^{IV}(dtc)_3]^+/Ni^{III}(dtc)_3$ redox couples (Figures 5b and S5), which suggests that irreversible decomposition of $[Ni^{III}(dtc)_2(py)_2]^+$ into $[Ni^{IV}(dtc)_3]^+$ must be occurring on the time scale of the CV experiment. We can therefore view the decomposition reaction as the rate-determining chemical step of an ECE/DISP mechanism, where the first E step is the pyridine-coupled oxidation to $[Ni^{III}(dtc)_2(py)_2]^+$ and the second E step is oxidation of the decomposition product to $[Ni^{IV}(dtc)_3]^+$.

The rate constant for decomposition (k_{dec}) was determined by evaluating the ratio of the cathodic-to-anodic peak currents (i_{pc}/i_{pa}) for the $[Ni^{III}(dtc)_2(py)_2]^+/Ni^{II}(dtc)_2$ wave.[54,63,64] A plot of i_{pc}/i_{pa} versus log(v) is shown in Figure 7a, where k_{dec} was determined using a working curve for an ECE/DISP mechanism generated using *DigiElch* software (Table S9). Values of k_{dec} over a range of pyridine concentrations are given in Table 1. For smaller values of k_{dec}, irreversibility (i_{pc}/i_{pa} = 0) of the redox wave is obtained at lower scan rates. As k_{dec} increases, the i_{pc}/i_{pa} curve shifts uniformly toward higher scan rates; thus, the potential must be scanned faster to obtain a quasi-reversible wave. Note that the reversible limit in Figure 7a occurs at i_{pc}/i_{pa} = 0.72. This is due to that fact that uncorrected peak currents were used for analysis in order to avoid errors in correcting for background, nonfaradic currents. Working curves were generated based on the same principle.

Table 1 shows that the decomposition rate constant decreases with higher [py], consistent with stabilization of $[Ni^{III}(dtc)_2(py)_2]^+$. Furthermore, the inverse dependence on pyridine indicates that decomposition of $[Ni^{III}(dtc)_2(py)_2]^+$ to yield $[Ni^{IV}(dtc)_3]^+$ must involve an equilibrium reaction that dissociates pyridine from the nickel metal center. Therefore, we propose that decomposition of $[Ni^{III}(dtc)_2(py)_2]^+$ occurs through two parallel reaction pathways: one in which dipyridine $[Ni^{III}(dtc)_2(py)_2]^+$ decays to $[Ni^{IV}(dtc)_3]^+$ and another in which monopyridine $[Ni^{III}(dtc)_2py]^+$ decays to $[Ni^{IV}(dtc)_3]^+$. The second pathway is controlled by the equilibrium constant between the di- and monopyridine-coordinated species shown in eq 16. If a steady-state approximation is made for the decay of $[Ni^{III}(dtc)_2py]^+$, then the parallel reaction scheme can be described by an overall k_{dec} given by eq 17. The rate constants k_2 and k_1 describe the decomposition of $[Ni^{III}(dtc)_2(py)_2]^+$ and $[Ni^{III}(dtc)_2py]^+$, respectively, while k_{+py} and k_{-py} describe the rate constants for pyridine coordination and dissociation, respectively, of the second pyridine ligand with Ni^{III}. A simplified expression can be obtained with $k_1' = k_1/K_{3,py2}$, where $K_{3,py2} = k_{+py}/k_{-py}$, which is suitable for fitting the data. A complete derivation of this expression is shown in the Supporting Information.

$$[Ni^{III}(dtc)_2(py)_2]^+ \rightleftharpoons [Ni^{III}(dtc)_2py]^+ + py \quad (16)$$

$$k_{dec} = k_2 + \frac{k_1 k_{-py}}{k_1 + k_{+py}[py]} = k_2 + \frac{k_1' k_{-py}}{k_1' + k_{-py}[py]} \quad (17)$$

Analysis of k_{dec} as a function of [py] is shown in Figure 7b, where the solid line represents a fit to eq 17. The extracted rate constants are k_2 = 0.54 s^{-1}, $k_1' = k_1/K_{3,py2}$ = 0.10 M s^{-1}, and

DOI: 10.1021/acs.inorgchem.9b02430
Inorg. Chem. XXXX, XXX, XXX−XXX

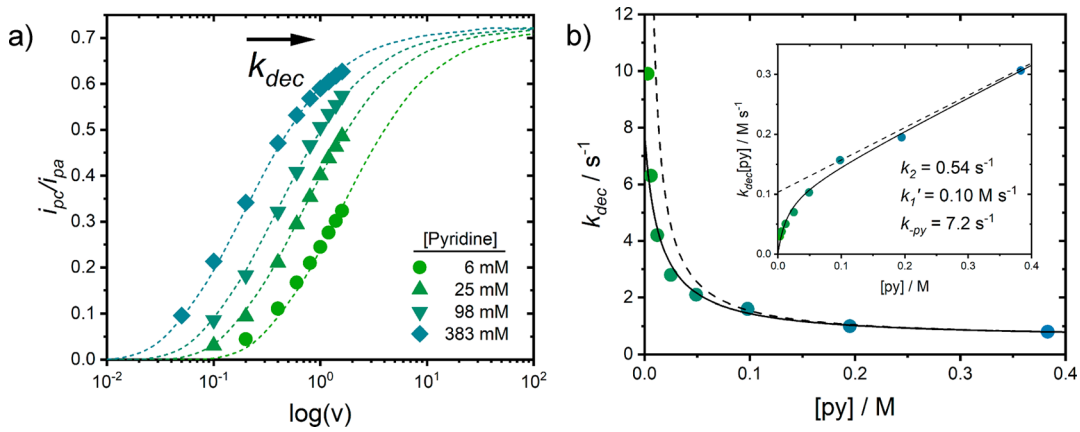

Figure 7. (a) Ratio of the cathodic-to-anodic peak currents associated with the $[Ni^{III}(dtc)_2(py)_2]^+/Ni^{II}(dtc)_2$ redox couple plotted versus log(v). The decomposition rate constant (k_{dec}) was determined for each [py] using the working curves (dashed lines) generated for an ECE/DISP mechanism. (b) Plot of k_{dec} versus [py] showing a decrease in k_{dec} for higher [py]. The solid overlaid line represents a fit to eq 17 with the rate constants given in the figure. The dashed overlaid line represents the limiting form of eq 17 at high [py]. The inset shows a plot of k_{dec}[py] versus [py] to highlight the linear dependence at high [py]. Overlaid lines are the same as those of the main figure.

k_{-py} = 7.2 s^{-1}. At a high pyridine concentration, eq 17 takes the limiting form $k_{dec} = k_2 + k_1'/[py]$. Multiplication by [py] allows for a linear expression to be obtained, $k_{dec}[py] = k_2[py] + k_1'$. Fits to these limiting expressions (k_{dec} and k_{dec}[py]) are shown as dashed lines in Figure 7b, with the inset plot highlighting the linear behavior at high [py]. As the pyridine concentration increases further, k_{dec} is expected to asymptotically approach k_2, representative of decomposition only through $[Ni^{III}(dtc)_2(py)_2]^+$.

The reductions of $[Ni^{IV}(dtc)_3]^+$ and $Ni^{III}(dtc)_3$ were not significantly impacted by the presence of pyridine, as shown by the similar cathodic peak positions compared to blank MeCN. Figure S4 shows a comparison of E_{pc}(III/II) versus log(v) for 0 and 383 mM pyridine concentrations. The slope for both plots is 38 mV dec^{-1}, indicating an EC mechanism, as described by eqs 10 and 11. Analysis of the rate constant for the chemical step in the presence of pyridine using eq 12 yields k_c(III/II) = 3.3 s^{-1}, an estimate similar to that obtained in blank MeCN.

Spectroelectrochemistry. The spectroelectrochemistry of $Ni^{II}(dtc)_2$ in MeCN with and without pyridine showed no evidence for the $[Ni^{III}(dtc)_2(py)_2]^+$ intermediate and instead showed only oxidation from $Ni^{II}(dtc)_2$ to $[Ni^{IV}(dtc)_3]^+$ in both cases. Figure S10a shows UV–vis absorption spectra of $Ni^{II}(dtc)_2$ collected as a function of the applied potential in the absence of pyridine. At increasingly positive applied potentials, decay of the $Ni^{II}(dtc)_2$ absorbance spectrum with λ_{max} = 388 nm gives rise to a broad increase in absorbance across the visible region with λ_{max} = 445 nm, consistent with the formation of $[Ni^{IV}(dtc)_3]^+$.[20] Figure S10b shows an identical experiment performed with [py] = 98 mM in which clean conversion from $Ni^{II}(dtc)_2$ to $[Ni^{IV}(dtc)_3]^+$ can be observed with no intermediate absorbance features. Conversion from $Ni^{II}(dtc)_2$ to $[Ni^{IV}(dtc)_3]^+$ occurred with $E_{1/2}$ = 0.10 V in the absence of pyridine and $E_{1/2}$ = −0.06 V in the presence of pyridine. This shift in $E_{1/2}$ was consistent with the CV results discussed above. The ultimate formation of $[Ni^{IV}(dtc)_3]^+$ in the spectroelectrochemical experiments is also consistent with the mechanism proposed from CV studies in which $[Ni^{III}(dtc)_2(py)_2]^+$ decays to $[Ni^{IV}(dtc)_3]^+$ at slow scan rates or, equivalently, long time scales. Notably, the concentration of $[Ni^{IV}(dtc)_3]^+$ produced in the absence of pyridine was larger than that produced in the presence of pyridine. We believe that this is likely due to the decomposition of $[Ni^{IV}(dtc)_3]^+$ into $Ni^{II}(dtc)_2$ and $(dtc)_2$ (thiuram disulfide) that has been reported to occur in the presence of pyridine and light.[33,34]

DISCUSSION

Oxidation/Reduction of $Ni^{II}(dtc)_2$ in the Absence of Pyridine. The multielectron redox cycle of $Ni^{II}(dtc)_2$ in MeCN can be described using the thermochemical cycle shown in Scheme 1. Horizontal arrows indicate 1e$^-$-transfer reactions and vertical arrows describe equilibria between bis- and tris-chelated nickel complexes, as stated in eq 18. According to Scheme 1, oxidation of $Ni^{II}(dtc)_2$ to $[Ni^{IV}(dtc)_3]^+$ must proceed through two 1e$^-$-transfer steps and one equilibrium. This may be achieved by three pathways: (1) sequential oxidation of $Ni^{II}(dtc)_2$ to $[Ni^{IV}(dtc)_2]^{2+}$, followed by ligand exchange to $[Ni^{IV}(dtc)_3]^+$ (i.e., $E_1^\circ \rightarrow E_2^\circ \rightarrow K_4$); (2) ligand exchange to $[Ni^{II}(dtc)_3]^-$ followed by sequential oxidation (i.e., $K_2 \rightarrow E_3^\circ \rightarrow E_4^\circ$); or (3) oxidation to $[Ni^{III}(dtc)_2]^+$, followed by ligand exchange to $Ni^{III}(dtc)_3$ and oxidation to $[Ni^{IV}(dtc)_3]^+$ (i.e., $E_1^\circ \rightarrow K_3 \rightarrow E_4^\circ$). The ECE/DISP mechanism described by eqs 4–7 constitutes pathway 3 and was originally proposed by Lachenal.[21]

Scheme 1. Thermochemical Cycle Describing the Multiple Electron-Transfer and Ligand-Transfer Reactions Involved in the $[Ni^{IV}(dtc)_3]^+/Ni^{II}(dtc)_2$ Redox Couple[a]

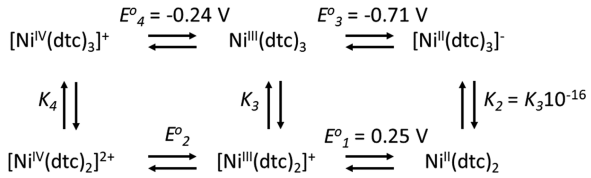

[a]The redox potentials are reported versus $Fc^{+/0}$.

$$2[Ni^x(dtc)_2]^{x-2} + Ni^{II}(dtc)_2 \underset{K_x}{\rightleftharpoons} 2[Ni^x(dtc)_3]^{x-1} + Ni^{II} \quad (18)$$

The standard redox potential E_1° = 0.25 V versus $Fc^{+/0}$ was estimated here using CV data collected at high scan rates. The

DOI: 10.1021/acs.inorgchem.9b02430
Inorg. Chem. XXXX, XXX, XXX−XXX

redox potentials of $E_3^\circ = -0.71$ V and $E_4^\circ = -0.24$ V were reported previously for electrochemical studies on $[Ni^{IV}(dtc)_3]^+$ and are consistent with the data presented here.[21] The potential E_2° for $[Ni^{IV}(dtc)_2]^{2+}/[Ni^{III}(dtc)_2]^+$ has not been previously reported and was not determined in the present study. We anticipate that this potential lies at an extremely positive voltage because of the unlikely formation of a four-coordinate Ni^{IV} complex. Almost all Ni^{IV} complexes reported in the literature are six-coordinate,[43−45,47−49,51,65−71] where only a few examples of lower coordination have been observed using bulky ligands that prevent higher coordination numbers.[72,73] Estimates of K_2, K_3, and K_4 are not available in the literature; however, the difference in E_3° and E_1° can be used to estimate the ratio of equilibrium constants $K_3/K_2 = 1.7 \times 10^{16}$ based on the relationship $(E_1^\circ - E_3^\circ) = (RT/F)\ln(K_3/K_2)$.

The scan-rate-dependent CV data presented here strongly support the ECE/DISP pathway. This is evidenced by the slopes of E_{pa}(IV/II) versus log(v) extracted from Figure 3b, which indicate regions of kinetic control by both chemical (∼30 mV dec^{-1}) and electrochemical (∼60 mV dec^{-1}) steps as well as the increase in the normalized peak current at low scan rates. The overall ligand-exchange reaction expressed in eq 5 indicates complexity of the reaction beyond a simple transfer of the dithiocarbamate ligand. Given that the only source for dtc$^-$ ligands in the electrolyte is $Ni^{II}(dtc)_2$, we propose that the first step in the overall ligand-exchange process is a reaction between $[Ni^{III}(dtc)_2]^+$ and $Ni^{II}(dtc)_2$, according to eq 19, to form a sulfur-bridged dimer, $[Ni_2(dtc)_4]^+$. Dithiocarbamate-bridged dimers have been observed previously, with the structures of the $[Co_2(dtc)_5]^+$ and $[Ru_2(dtc)_5]^+$ dimers characterized to show bridging sulfur atoms, which also chelate to the metal centers.[32,74−76] Ligand-exchange reactions between Fe^{III}, Ni^{II}, and Hg^{II} complexes containing different dithiocarbamate derivatives have also been well documented and proposed to occur through dimer intermediates.[32] The ultimate fate of the proposed $[Ni_2(dtc)_4]^+$ dimer must be the generation of $Ni^{III}(dtc)_3$ and free Ni^{II} ions according to eq 5. We speculate that the dimer may dissociate via eq 20 to yield $Ni^{III}(dtc)_3$ and $[Ni^{II}(dtc)]^+$. The resulting $[Ni^{II}(dtc)]^+$, likely coordinated to MeCN, may then undergo disproportionation to yield free Ni^{II} ions and $Ni^{II}(dtc)_2$ (eq 21).

$$[Ni^{III}(dtc)_2]^+ + Ni^{II}(dtc)_2 \rightarrow [Ni_2(dtc)_4]^+ \quad (19)$$

$$[Ni_2(dtc)_4]^+ \rightarrow Ni^{III}(dtc)_3 + [Ni^{II}(dtc)]^+ \quad (20)$$

$$2[Ni^{II}(dtc)]^+ \rightarrow Ni^{II}(dtc)_2 + Ni^{II} \quad (21)$$

The consumption of a sacrificial $Ni^{II}(dtc)_2$ molecule during the ECE/DISP pathway further classifies this reaction as a radical substrate dimerization mechanism, for which there are numerous examples, especially related to organic radicals.[54,56−58] For the specific case of an RSD-ECE/DISP pathway, Saveant has shown that the rate constant for the chemical step can be defined further by the relationship $k_c = 4k_{LE}[Ni^{II}(dtc)_2]_0$ or $k_c = 2k_{LE}[Ni^{II}(dtc)_2]_0$, where k_{LE} is the second-order rate constant for the ligand-exchange reaction.[54,56] The former expression refers to the case where k_{LE} is larger than the disproportionation rate constant (k_D) and represents a true ECE mechanism, where $Ni^{III}(dtc)_3$ is oxidized quickly at the electrode surface. The latter expression is reserved for the case where $k_D > k_{LE}$ and represents a DISP1 mechanism. Using $k_c = 34$ s^{-1} and $[Ni^{II}(dtc)_2]_0 = 1$ mM, $k_{LE} =$ 8500 M^{-1} s^{-1} if an ECE pathway is operative and $k_{LE} = 17000$ M^{-1} s^{-1} if a DISP1 pathway is operative. Notably, a third possibility may occur where ligand exchange occurs as a preequilibrium to disproportionation. This mechanism is referred to as a DISP2 pathway and exhibits a characteristic E_{pa} versus log(v) slope of 19.7 mV dec^{-1}. Given the observed 29 mV dec^{-1} slope, the DISP2 pathway was not considered further.

Distinguishing between an ECE and DISP1 pathway can be very difficult without knowledge of k_D. The disproportionation reaction described by eq 7 arises from the difference in the redox potentials for the two intermediate Ni^{III} species, $[Ni^{III}(dtc)_2]^+$ and $Ni^{III}(dtc)_3$. Using the reduction potentials in Scheme 1, $\Delta G_{DISP}^\circ = -nF(E_1^\circ - E_4^\circ) = -0.49$ eV can be calculated. We note that, given the bridging nature of dithiocarbamate ligands, this reaction may proceed through an inner- or outer-sphere pathway. The large driving force of the disproportionation step highlights the impact of ligand coordination in determining the redox potential of the metal center. For example, coordination of a third dtc$^-$ ligand to Ni^{III} results in a shift of 0.96 V in the $Ni^{III/II}$ reduction potential from the bis- to tris-coordinated species. This large difference in the potentials allows for a potential inversion between E_1° and E_4°, resulting in thermodynamically favorable disproportionation. The key to the observed 2e$^-$ oxidation from $Ni^{II}(dtc)_2$ to $[Ni^{IV}(dtc)_3]^+$ is therefore the large difference in the equilibrium constants for ligand exchange, K_2 and K_3. An estimate of K_2 has never been measured in the literature, likely because of its extremely small magnitude, and $[Ni^{II}(dtc)_3]^-$ has never been isolated and characterized. The instability of this species is due to the strong preference of Ni^{II} toward a square-planar geometry when coordinated to dithiocarbamate ligands as a result of its d^8 electronic configuration and strong π donation from the conjugated ligand.[38] Notably, $[Fe(dtc)_3]^-$ (d^6) and $[Co(dtc)_3]^-$ (d^7) are stable complexes, and CV studies exhibit sequential 1e$^-$ waves for their $M^{IV/III}$ and $M^{III/II}$ redox couples.[77,78]

On the other end of the redox cycle, Ni^{IV} is present in a six-coordinate environment with a low-spin electronic configuration.[34] Other known examples of Ni^{IV} complexes also exhibit low-spin, six-coordinate geometries.[43−45,49,52] Therefore, the equilibrium constant K_4 in Scheme 1 is expected to be extremely large. Considering Scheme 1 as a whole, we can see that $K_4 \gg K_3 \gg K_2$ and the regions of stability are tilted toward the corners of $Ni^{II}(dtc)_2$ and $[Ni^{IV}(dtc)_3]^+$. The equilibrium K_3 is then critical to the ability to facilitate 1e$^-$ versus 2e$^-$ reactions. If $K_3 \ll 1$, only the 1e$^-$ $[Ni^{III}(dtc)_2]^+/Ni^{II}(dtc)_2$ process would be observed; however, if $K_3 \gg 1$, then the ECE mechanism described above would proceed.

The reduction of $[Ni^{IV}(dtc)_3]^+$ back to $Ni^{II}(dtc)_2$ during CV experiments occurs predominately through sequential 1e$^-$-transfer reactions, followed by equilibration of $[Ni^{II}(dtc)_3]^-$ to $Ni^{II}(dtc)_2$ (i.e., $E_4^\circ \rightarrow E_3^\circ \rightarrow K_2$ from Scheme 1). This is due to the relative stability of the tris-chelated $Ni^{III}(dtc)_3$ complex. However, the notable difference in the peak currents for the two redox waves suggests some degree of instability. Lachenal proposed that the instability of $Ni^{III}(dtc)_3$ was due to an internal decomposition via oxidation of a dtc$^-$ ligand to yield $Ni^{II}(dtc)_2$ and $(dtc)_2$.[21] Controlled potential electrolysis of $[Ni^{IV}(dtc)_3]^+$ at a potential between E_4° and E_3° indeed revealed the ultimate production of $Ni^{II}(dtc)_2$ and $(dtc)_2$. However, this reaction involved the reduction of a $[Ni^{IV}(dtc)_3]^+$ starting material and would necessarily produce

DOI: 10.1021/acs.inorgchem.9b02430
Inorg. Chem. XXXX, XXX, XXX−XXX

uncoordinated dithiocarbamate species.[21] Electrochemical studies presented here with Na(dtc) added to $Ni^{II}(dtc)_2$ solutions showed that the irreversible oxidation of dtc^- to $dtc^\bullet$ gave rise to an increase in the current for the oxidation of $Ni^{III}(dtc)_3$ to $[Ni^{IV}(dtc)_3]^+$. Such an increase indicates that spontaneous and kinetically fast oxidation of $Ni^{II}(dtc)_2$ by $dtc^\bullet$ occurs in a homogeneous solution to generate $Ni^{III}(dtc)_3$. This reaction is formally the reverse of that proposed by Lachenal and clearly indicates favorability in the formation of $Ni^{III}(dtc)_3$, not decomposition.

In the present case, where the oxidation of $Ni^{II}(dtc)_2$ is followed by the reduction of $[Ni^{IV}(dtc)_3]^+$ on the return scan, decomposition of $Ni^{III}(dtc)_3$ must occur on the time scale of the CV experiment. We propose that this happens via a reaction between $Ni^{III}(dtc)_3$ and Ni^{II} ions liberated during the oxidation step to regenerate $[Ni^{III}(dtc)_2]^+$. Formally, this reaction is the reverse of the ligand-exchange step shown in eq 5. Production of $[Ni^{III}(dtc)_2]^+$ then results either in reduction at the electrode surface where the applied potential is now less than $E_1°$ or through the disproportionation reaction described in eq 7.

Oxidation/Reduction of $Ni^{II}(dtc)_2$ in the Presence of Pyridine. The addition of pyridine to the MeCN solution resulted in a shift of the $Ni^{II}(dtc)_2$ oxidation peak in the negative direction and an increase in the reversibility. The pyridine-coupled redox feature can best be described as a $[Ni^{III}(dtc)_2(py)_2]^+/Ni^{II}(dtc)_2$ redox couple where the equilibrium constant for pyridine coordination to $[Ni^{III}(dtc)_2]^+$ was determined to be $K = 1.4\ (\pm 0.2) \times 10^6\ M^{-2}$. The negative shift in $E_{pa}(III_{py}/II)$ is characteristic of ligand-coupled electron transfer (LCET). The LCET process is analogous to proton-coupled electron transfer (PCET) in which the reduction of a molecule is coupled with proton transfer in order to stabilize the more electron-rich reduced species. A characteristic result of PCET is a positive shift in the cathodic peak potential for increased $[H^+]$. In the case of $Ni^{II}(dtc)_2$ oxidation, the electron density from the coordinated pyridine ligands is necessary to stabilize the electron-deficient Ni^{III} metal center. Because of this stabilization effect with added [py], a negative shift in E_{pa} is observed, indicating that oxidation is easier in the presence of pyridine.

Scheme 2 summarizes the effect of pyridine coordination on the $Ni^{III/II}$ reduction potential. Here, the equilibrium constants for pyridine coordination to $[Ni^{III}(dtc)_2]^+$ are described by $K_{3,py1}$ and $K_{3,py2}$, of which the product $K_{3,py1}K_{3,py2} = K = 1.4\ (\pm 0.2) \times 10^6\ M^{-2}$. The equilibrium constants for pyridine coordination to $Ni^{II}(dtc)_2$ are smaller than we can detect using UV–vis and ^1H NMR methods; however, the overall equilibrium $K_{2,py1}K_{2,py2} = 0.087\ M^{-2}$ has been measured using the magnetic susceptibility in a mixture of 95% pyridine, 2.5% CH_2Cl_2, and 2.5% *tert*-butyl alcohol.[62] The small magnitude for pyridine coordination is attributed to the strong square-planar coordination environment induced by the dithiocarbamate ligands and has been noted previously in the literature.[38] Coordination of other nitrogen bases such as 1,10-phenanthroline and *n*-hexylamine to $Ni^{II}(dtc)_2$ have also been noted in the literature, with the chelating 1,10-phenanthroline (phen) yielding a significantly higher equilibrium constant ($K_{phen} = 2240\ M^{-1}$) because of the formation of a cis-coordinated adduct.[79,80] Using the literature value for the formation of $Ni^{II}(dtc)_2(py)_2$ and the value measured here for the formation of $[Ni^{III}(dtc)_2(py)_2]^+$, we can estimate the redox potential of $E_{py2}° = -0.18$ V based on Scheme 2. The magnitude of $E_{py1}°$ is still unknown without knowledge of the individual equilibrium constants for pyridine coordination ($K_{3,py1}$, $K_{3,py2}$, $K_{2,py1}$, and $K_{2,py2}$).

We can estimate that the concentration of $Ni^{II}(dtc)_2(py)_2$ over the range of 0–383 mM pyridine never exceeds 0.013 mM or 1.3% of Ni^{II} species based on $K_{2,py1}K_{2,py2} = 0.087\ M^{-2}$. This indicates that the pyridine-coupled oxidation observed by CV mostly occurs through an ECC process ($E_1° \rightarrow K_{3,py1} \rightarrow K_{3,py2}$), with pyridine coordination to $[Ni^{III}(dtc)_2]^+$ occurring after oxidation. The reduction of $[Ni^{III}(dtc)_2(py)_2]^+$ to $Ni^{II}(dtc)_2$ may occur through either the reduction of $Ni^{II}(dtc)_2(py)_2$ followed by rapid dissociation of pyridine ligands (ECC mechanism; $E_{py2}° \rightarrow K_{2,py2} \rightarrow K_{2,py1}$) or through pyridine dissociation followed by the reduction of $[Ni^{III}(dtc)_2py]^+$ to $Ni^{II}(dtc)_2py$ before loss of the second pyridine (CEC mechanism; $K_{3,py2} \rightarrow E_{py1}° \rightarrow K_{2,py1}$).

The structure of the $[Ni^{III}(dtc)_2(py)_2]^+$ complex is presently unknown, but we can speculate that the species exists in a six-coordinate environment with either a cis or trans conformation (Figure 8). The reversibility of the pyridine-coupled wave at high scan rates could indicate that a trans conformation is favored, resulting in a lower energy barrier for pyridine coordination, where the dithiocarbamate ligand framework would not undergo significant reorganization. However, the cis form is more similar to the ultimate structure of $[Ni^{IV}(dtc)_3]^+$, which exists in a tris-chelated octahedral environment. We note that theoretical calculations for the coordination of ethylamine to $Ni^{II}(dtc)_2$ have indicated that the trans isomer is 7.19 kcal mol^{-1} more favorable.[80]

Scheme 2. Thermochemical Cycle Describing $Ni^{III/II}$ Reduction Potentials as a Function of Pyridine Coordination

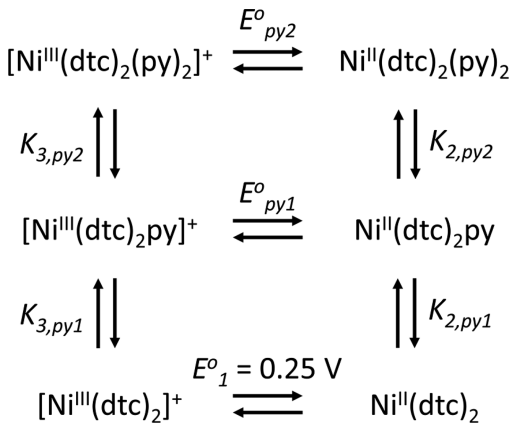

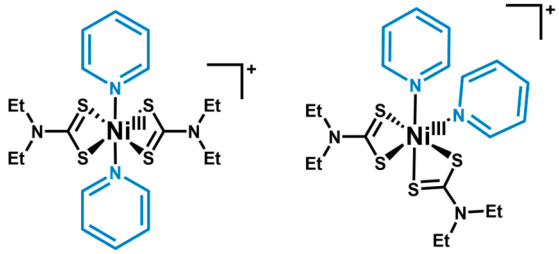

Figure 8. Proposed trans- and cis-octahedral structures for $[Ni^{III}(dtc)_2(py)_2]^+$.

DOI: 10.1021/acs.inorgchem.9b02430
Inorg. Chem. XXXX, XXX, XXX–XXX

The instability of the $[Ni^{III}(dtc)_2(py)_2]^+$ complex at low scan rates resulted in voltammograms that strongly resembled those without pyridine but with a shifted anodic wave. The consistency in the appearance of $1e^-$ reduction waves for $[Ni^{IV}(dtc)_3]^+$ and $Ni^{III}(dtc)_3$ at low scan rates and the spectroelectrochemical data that show the ultimate formation of $[Ni^{IV}(dtc)_3]^+$ indicate that $[Ni^{III}(dtc)_2(py)_2]^+$ must decompose to $[Ni^{IV}(dtc)_3]^+$. The rate constant for this reaction was measured using the ratio of cathodic-to-anodic peak currents versus scan rate, where the dependence of k_{dec} on the pyridine concentration was well described by a parallel decay mechanism. The two reactions are proposed to be decomposition via $[Ni^{III}(dtc)_2(py)_2]^+$ or $[Ni^{III}(dtc)_2py]^+$. Within the context of the ligand-exchange mechanism outlined above for the absence of pyridine, we speculate that the decay of $[Ni^{III}(dtc)_2(py)_2]^+$ and $[Ni^{III}(dtc)_2py]^+$ yields $Ni^{III}(dtc)_3$ as the initial decomposed product. This is reasoned based on the fact that ligand exchange must certainly be present in order to form a tris-chelated nickel complex and $Ni^{III}(dtc)_3$ would provide a direct precursor to $[Ni^{IV}(dtc)_3]^+$.

Scheme 3 offers a summary of these reaction pathways in relation to the ECE/DISP mechanism outlined in blank MeCN. Following oxidation from $Ni^{II}(dtc)_2$ to $[Ni^{III}(dtc)_2]^+$, rapid coordination of pyridine prevents the ligand-exchange reaction, which occurs in blank MeCN with a rate constant of 17000 M^{-1} s^{-1}. Instead, the formation of $[Ni^{III}(dtc)_2py]^+$ and $[Ni^{III}(dtc)_2(py)_2]^+$ result in partially stable coordination complexes with much slower rate constants for conversion to $Ni^{III}(dtc)_3$. The apparent first-order rate constants for $[Ni^{III}(dtc)_2py]^+$ and $[Ni^{III}(dtc)_2(py)_2]^+$ decomposition were measured to be $k_1 = 0.1K_{3,py2}$ s^{-1} and $k_2 = 0.54$ s^{-1}. Although a $Ni^{II}(dtc)_2$ concentration dependence was not performed, conversion of these values to second-order rate constants based on $[Ni^{II}(dtc)_2]_0 = 1$ mM results in $k_1' = 100K_{3,py2}$ M^{-1} s^{-1} and $k_2' = 540$ M^{-1} s^{-1}. The parallel decay mechanism points to a small equilibrium constant for coordination of the second pyridine. A reasonable estimate of $K_{3,py2} < 10$ M^{-1} thus results in $k_1' < 1000$ M^{-1} s^{-1}. The rate constants k_1' and k_2' are therefore much smaller than k_{LE} and justify the quasi-reversible electrochemistry observed for $[Ni^{III}(dtc)_2(py)_2]^+$. The product of each ligand-exchange reaction is proposed to be $Ni^{III}(dtc)_3$, which could undergo further oxidation to $[Ni^{IV}(dtc)_3]^+$ either at the electrode surface or through a disproportionation reaction in solution. Additional disproportionation reactions emerge in the presence of pyridine because of the multiple pyridine-coordinated Ni^{III} species. These are described generally by the DISP reaction in Scheme 3.

Scheme 3. Proposed ECE/DISP Mechanism Describing the Oxidation of $Ni^{II}(dtc)_2$ to $[Ni^{IV}(dtc)_3]^+$ in the Presence of Pyridine

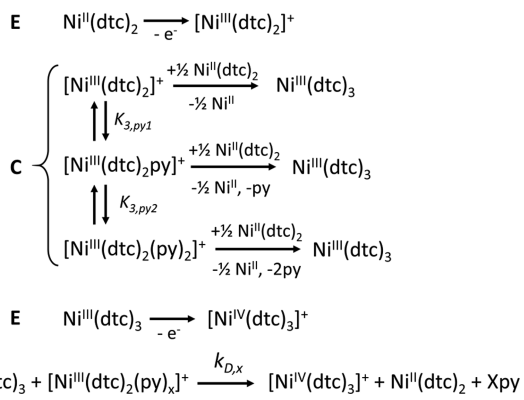

Digital Simulations of the CV Data. In order to fully describe the complex redox cycle for the $[Ni^{IV}(dtc)_3]^+/Ni^{II}(dtc)_2$ couple in MeCN with and without pyrdine, we have used digital simulation software (*DigiElch*) to model the experimental CV data as a function of the scan rate based on Schemes 1−3. In the case of MeCN only, known redox potentials $E_1°$, $E_3°$, and $E_4°$ were held constant in addition to the rate constants for electron transfer $k_E = 0.018$ cm s^{-1}, determined here for the $[Ni^{III}(dtc)_2]^+/Ni^{II}(dtc)_2$ redox couple, and $k_{LE} = 17000$ M^{-1} s^{-1} associated with a DISP1 mechanism. A detailed description of the fitting procedure is provided in the Supporting Information. Figure 9a shows a comparison of the experimental cyclic voltammograms for 1 mM $Ni^{II}(dtc)_2$ at 100 and 1000 mV s^{-1} with simulations overlaid as dashed lines. The agreement between the simulations and the experimental data is excellent with only small differences in the region of the $Ni^{III}(dtc)_3/Ni^{II}(dtc)_2$ peak. Importantly, the simulations model the changes in E_{pa}(IV/II), i_{pa}(IV/II), and i_{pc}(III/II) as a function of the scan rate quite well.

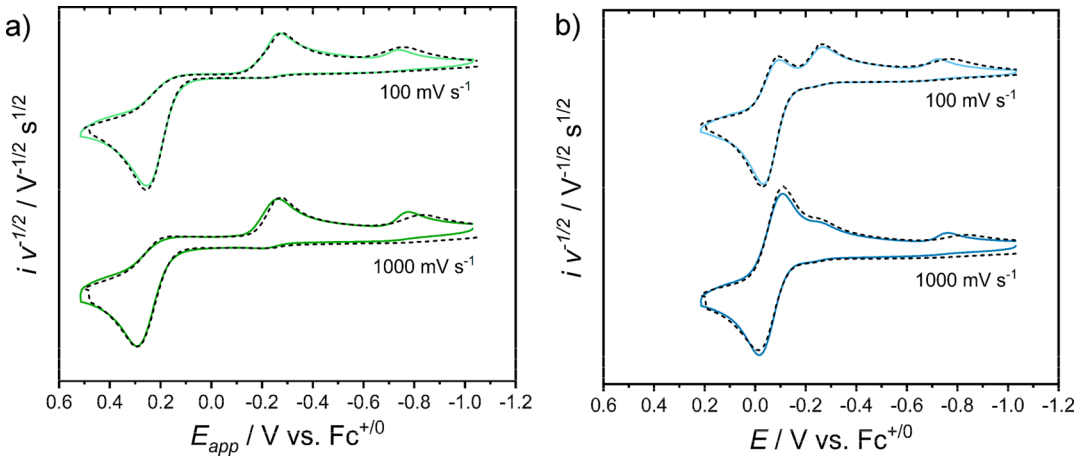

Figure 9. Comparison of the experimental (solid lines) and simulated (black dashed lines) CV data collected for $Ni^{II}(dtc)_2$ in (a) MeCN and (b) MeCN with 383 mM pyridine at 100 and 1000 mV s^{-1}.

DOI: 10.1021/acs.inorgchem.9b02430
Inorg. Chem. XXXX, XXX, XXX−XXX

On the basis of these simulations, an equilibrium constant for eq 5 of K_3 = 0.079 was calculated. From this value, an estimate of K_2 = 4.6 × 10^{-18} can be reasonably made. The magnitude of K_3 indicates that ligand exchange between $[Ni^{III}(dtc)_2]^+$ and $Ni^{II}(dtc)_2$ is slightly disfavored. We would have expected that K_3 > 1 based on the observed 2e$^-$ oxidation and 1e$^-$ reduction processes; however, 2e$^-$ oxidation may still proceed if k_d is sufficiently fast.[54] Indeed, the disproportionation rate constant was best simulated near the diffusion limit and was therefore held constant at 1 × 10^{10} M^{-1} s^{-1}. The large magnitude of this estimate is consistent with the large driving force for disproportionation and supports our use of k_{LE} = 17000 M^{-1} s^{-1} (DISP1 pathway) in the simulations. The fact that K_3 is close to 1 is consistent with our proposal of $Ni^{III}(dtc)_3$ decomposition through ligand exchange/disproportionation prior to being reduced at $E_3°$ = −0.71 V. Additionally, CV data were collected with only $Ni^{II}(dtc)_2$ present in the solution and no added Ni^{II} ions to balance the equilibrium. Therefore, the only Ni^{II} ions in solution are produced as a result of oxidation, the low concentration of which may skew the equilibrium toward the favorable formation of $Ni^{III}(dtc)_3$. This suggests that the addition of Ni^{II} ions to solution may have a pronounced effect on CV. Studies of this nature are currently under investigation in our laboratory.

Figure 9b shows digital simulations overlaid with the experimental CV data collected with [py] = 383 mM. All experimentally obtained rate constants, reduction potentials, and equilibrium constants were fixed during simulations, while unknown values were allowed to float to obtain a best fit. The proposed model agrees well with the experimental data but misses some in the region of the $Ni^{III}(dtc)_3/Ni^{II}(dtc)_2$ peak, similar to what was observed in the absence of pyridine. A further understanding of this reduction step is needed in order to refine the model for better fitting in this region. Regardless, the model does an excellent job of fitting the change in reversibility of the $[Ni^{III}(dtc)_2(py)_2]^+/Ni^{II}(dtc)_2$ couple as a function of the scan rate.

Given the complexity of the mechanism proposed in Scheme 3 and the limited amount of known thermodynamic and kinetic information, the errors associated with the fitting parameters such as the equilibrium and rate constants are much greater than what was found in the absence of pyridine. Nonetheless, the simulations provide support for a small equilibrium constant between $[Ni^{III}(dtc)_2(py)_2]^+$ and $[Ni^{III}(dtc)_2py]^+$. The best fit to the experimental data resulted in equilibrium constants for pyridine coordination of $K_{3,py1}$ = 2.5 × 10^5 M^{-1} and $K_{3,py2}$ = 2 M^{-1}, with their product $K_{3,py1}K_{3,py2}$ = 5 × 10^5 M^{-2} being close to the experimental value of 1.4 (±0.2) × 10^6 M^{-2}. The large disparity in equilibria supports the observation that decomposition of $[Ni^{III}(dtc)_2(py)_2]^+$ occurs through two parallel pathways in which dissociation of a pyridine ligand to form $[Ni^{III}(dtc)_2py]^+$ is an important feature.

CONCLUSION

Here we have reported on the impact of pyridine coordination on the multielectron redox cycle of $Ni^{II}(dtc)_2$, where dtc$^-$ is *N*,*N*-diethyldithiocarbamate. A comparison of the electrochemical data in the absence and presence of pyridine reveals a common mechanism for 2e$^-$ oxidation from $Ni^{II}(dtc)_2$ to $[Ni^{IV}(dtc)_3]^+$ based on the RSD-ECE/DISP pathway. Using CV, we have uncovered a complex mechanism that involves pyridine coordination in the Ni^{III} oxidation state, which kinetically inhibits further oxidation to $[Ni^{IV}(dtc)_3]^+$. Organometallic nickel complexes reported by Sanford and Mirica have shown similar behavior, where scorpionate ligands have been used to rapidly coordinate and stabilize Ni^{III} upon 1e$^-$ oxidation from Ni^{II}.[45,46,49,50,52] Controlling this chemistry has led to both 1e$^-$ and 2e$^-$ catalytic pathways. In the case of nickel dithiocarbamates, both ligand coordination and reorganization of the ligand framework appear to be important in driving the overall 2e$^-$ oxidation from Ni^{II} to Ni^{IV}. Coordination of pyridine alone does not lead to potential inversion of the $Ni^{IV/III}$ and $Ni^{III/II}$ redox potentials, instead displaying 1e$^-$ redox chemistry through stabilization of Ni^{III}. The ultimate formation of $[Ni^{IV}(dtc)_3]^+$ even in the presence of pyridine shows that nickel dithiocarbamate bonding is still greatly favored and rearrangement of the ligand framework to a cis-octahedral environment is a significant factor in driving 2e$^-$ oxidation. Further studies are underway using derivatized pyridine ligands to enhance the stability of $[Ni^{III}(dtc)_2(py)_2]^+$ in order to slow down conversion to $[Ni^{IV}(dtc)_3]^+$ and produce isolable Ni^{III} complexes for structural study.

ASSOCIATED CONTENT

Supporting Information

The Supporting Information is available free of charge on the ACS Publications website at DOI: 10.1021/acs.inorgchem.9b02430.

CV, UV−vis absorbance, ^{1}H NMR, and EPR, and CV simulation data (PDF)

AUTHOR INFORMATION

Corresponding Author

*E-mail: farnum@auburn.edu.

ORCID

Byron H. Farnum: 0000-0001-9152-1909

Notes

The authors declare no competing financial interest.

ACKNOWLEDGMENTS

This work was supported by startup funds provided by Auburn University. The authors thank Eduardus Duin for help with EPR measurements.

REFERENCES

(1) Collman, J. P.; Rothrock, R. K.; Finke, R. G.; Moore, E. J.; Rose-Munch, F. Role of the Metal-Metal Bond in Transition-Metal Clusters. Phosphido-Bridged Diiron Carbonyl Complexes. *Inorg. Chem.* **1982**, *21* (1), 146−156.

(2) Van der Linden, J. G. M.; Paulissen, M. L. H.; Schmitz, J. E. J. Electrochemical Reduction of the Gold Cluster Au9(PPh3)83+. Evidence for an ErErCr Mechanism. Formation of the Paramagnetic Gold Cluster Au9(PPh3)82+. *J. Am. Chem. Soc.* **1983**, *105* (7), 1903−1907.

(3) Uhrhammer, D.; Schultz, F. A. Energetics of Concerted Two-Electron Transfer and Metal−Metal Bond Cleavage in Phosphido-Bridged Molybdenum and Tungsten Carbonyl Complexes. *J. Phys. Chem. A* **2002**, *106* (47), 11630−11636.

(4) Smith, D. A.; Zhuang, B.; Newton, W. E.; McDonald, J. W.; Shultz, F. A. Two-Electron Transfer Accompanied by Metal-Metal Bond Formation. Synthesis and Electrochemistry of Dinuclear Molybdenum and Tungsten Carbonyl Thiolates. *Inorg. Chem.* **1987**, *26* (15), 2524−2531.

DOI: 10.1021/acs.inorgchem.9b02430
Inorg. Chem. XXXX, XXX, XXX−XXX

(5) Zhuang, B.; McDonald, J. W.; Schultz, F. A.; Newton, W. E. Synthesis, Reactivity and Two-Electron Electrochemistry of the Dinuclear Molybdenum(0) Complexes [Et4N]2[Mo2(CO)8(SR)2] (R = Tert-Bu, Ph). *Organometallics* **1984**, *3* (6), 943−945.

(6) Hollis, L. S.; Lippard, S. J. Redox Properties of Cis-Diammineplatinum Alpha-Pyridone Blue and Related Complexes. Synthesis, Structure, and Electrochemical Behavior of Cis-Diammineplatinum(III) Dimers with Bridging.Alpha.-Pyridonate Ligands. *Inorg. Chem.* **1983**, *22* (18), 2605−2614.

(7) DiMaio, A.-J.; Rheingold, A. L.; Chin, T. T.; Pierce, D. T.; Geiger, W. E. Electrochemical and Structural Characterization of *Cis* - and *Trans* -[Cp(CO)Ru(μ-As(C_6H_5)$_2$)]$_2$, Isomers That Undergo Two-Electron-Transfer Oxidations †. *Organometallics* **1998**, *17* (6), 1169−1176.

(8) Sudha, C.; Mandal, S. K.; Chakravarty, A. R. Electrochemical Evidence for a Two-Electron Reduction Process in a (.Mu.-Oxo)Bis(.Mu.-Acetato)Diruthenium(III) Complex Containing Terminal 1-Methylimidazole Ligands. *Inorg. Chem.* **1993**, *32* (18), 3801−3802.

(9) Fernandes, J. B.; Zhang, L. Q.; Schultz, F. A. Correlation of Heterogeneous Electron Transfer Rate with Structural Change and Environmental Factors in the Two-Electron Oxidation of W2(CO) &pSBz) i-. *J. Electroanal. Chem. Interfacial Electrochem.* **1991**, *297*, 145−161.

(10) Hill, M. G.; Rosenhein, L. D.; Mann, K. R.; Mu, X. H.; Schultz, F. A. IR Spectroelectrochemical Investigation of the Disproportionation of Bis(Benzenemethanethiolato)Octacarbonylditungstate(2-). *Inorg. Chem.* **1992**, *31* (20), 4108−4111.

(11) Collins, B. E.; Koide, Y.; Schauer, C. K.; White, P. S. Structures, Bonding, Infrared Spectroscopy, and Two-Electron Reduction Potentials of the Coordinated Metallopnictanes $Fe_3(CO)_9(\mu_3$-$EML_n)_2$ (E = P, As, Sb; ML_n = $Cr(CO)_5$, $MnCp(CO)_2$). *Inorg. Chem.* **1997**, *36* (27), 6172−6183.

(12) Koide, Y.; Bautista, M. T.; White, P. S.; Schauer, C. K. Triiron-Triangle Opening and Closing by a Single Two-Electron Process in the Bicapped Triiron Clusters Fe3(CO)9(.Mu.3-PMLn)2 (MLn = CpFe(CO)2, CpMn(CO)2). *Inorg. Chem.* **1992**, *31* (18), 3690−3692.

(13) Edwin, J.; Geiger, W. E. Structural Consequences of Electron Transfer Reactions. 21. Structural Changes Coupled to Two-Electron-Transfer Reactions: Oxidation Mechanism of Pseudo-Triple-Decker Complexes of Cobalt and Rhodium. *J. Am. Chem. Soc.* **1990**, *112* (20), 7104−7112.

(14) Chin, T. T.; Geiger, W. E.; Rheingold, A. L. Relation of Structural Changes to Electron-Transfer Parameters in Fulvalenediyl Dirhodium Complexes Demonstrating Quasi-Reversible Two-Electron Voltammetry †. *J. Am. Chem. Soc.* **1996**, *118* (21), 5002−5010.

(15) Bowyer, W. J.; Geiger, W. E. Structural Consequences of Electron-Transfer Reactions. 11. Electrochemically Induced Changes in Hapticity in Mixed-Sandwich Compounds of Iridium and Rhodium. *J. Am. Chem. Soc.* **1985**, *107* (20), 5657−5663.

(16) Tulyathan, B.; Geiger, W. E. Structural Consequences of Electron-Transfer Reactions. Part 12. Multi Electron Processes Involving Structural Changes. The Two-Electron Reduction of Hexaosmium Carbonyl Cluster (Os6(CO)18). *J. Am. Chem. Soc.* **1985**, *107* (21), 5960−5967.

(17) Reingold, J. A.; Virkaitis, K. L.; Carpenter, G. B.; Sun, S.; Sweigart, D. A.; Czech, P. T.; Overly, K. R. Chemical and Electrochemical Reduction of Polyarene Manganese Tricarbonyl Cations: Hapticity Changes and Generation of *Syn* - and *Anti* -Facial Bimetallic η^4, η^6 -Naphthalene Complexes. *J. Am. Chem. Soc.* **2005**, *127* (31), 11146−11158.

(18) Waldie, K. M.; Ramakrishnan, S.; Kim, S.-K.; Maclaren, J. K.; Chidsey, C. E. D.; Waymouth, R. M. Multielectron Transfer at Cobalt: Influence of the Phenylazopyridine Ligand. *J. Am. Chem. Soc.* **2017**, *139* (12), 4540−4550.

(19) Chirik, P. J.; Wieghardt, K. Radical Ligands Confer Nobility on Base-Metal Catalysts. *Science* **2010**, *327* (5967), 794−795.

(20) Hendrickson, A. R.; Martin, R. L.; Rohde, N. M. Dithiocarbamates of Nickel in the Formal Oxidation States I-IV. Electrochemical Study. *Inorg. Chem.* **1975**, *14* (12), 2980−2985.

(21) Lachenal, D. Electrochemical Behaviour of Nickel (II) and Ni (IV) N,N-Diethyldithiocarbamates. Synthesis of a Nickel(IV) Species. *Inorg. Nucl. Chem. Lett.* **1975**, *11* (2), 101−106.

(22) Bartlett, P. N.; Eastwick-Field, V. A Reinvestigation of the Electrochemistry of [Ni(II)(Bpy)3(ClO)4)2] in Acetonitrile Using Rotating Disc and Rotating Ring-Disc Electrodes. *Electrochim. Acta* **1993**, *38* (17), 2515−2523.

(23) Sampson, M. D.; Nguyen, A. D.; Grice, K. A.; Moore, C. E.; Rheingold, A. L.; Kubiak, C. P. Manganese Catalysts with Bulky Bipyridine Ligands for the Electrocatalytic Reduction of Carbon Dioxide: Eliminating Dimerization and Altering Catalysis. *J. Am. Chem. Soc.* **2014**, *136* (14), 5460−5471.

(24) Ghosh, P.; Samanta, S.; Roy, S. K.; Joy, S.; Krämer, T.; McGrady, J. E.; Goswami, S. Redox Noninnocence in Coordinated 2-(Arylazo)Pyridines: Steric Control of Ligand-Based Redox Processes in Cobalt Complexes. *Inorg. Chem.* **2013**, *52* (24), 14040−14049.

(25) Sengupta, D.; Ghosh, P.; Chatterjee, T.; Datta, H.; Paul, N. D.; Goswami, S. Ligand-Centered Redox in Nickel(II) Complexes of 2-(Arylazo)Pyridine and Isolation of 2-Pyridyl-Substituted Triaryl Hydrazines via Catalytic N-Arylation of Azo-Function. *Inorg. Chem.* **2014**, *53* (22), 12002−12013.

(26) Lee, S.; Lovelace, S. R.; Arford, D. J.; Geib, S. J.; Weber, S. G.; Cooper, N. J. Reductively Induced Dimerization of the Ligated Benzene in [Mn(H6-C6H6)(CO)3]+: Formation of the Initial C−C Bond by Anion/Cation Addition. *J. Am. Chem. Soc.* **1996**, *118* (17), 4190−4191.

(27) Pierce, D. T.; Geiger, W. E. Structural Consequences of Electron-Transfer Reactions. Part XX. Splitting of a Two-Electron Cyclic Voltammetric Wave into Its One-Electron Components: The (.Eta.-C6Me6)2Ru2+/+/0) Couples. *J. Am. Chem. Soc.* **1989**, *111* (19), 7636−7638.

(28) Pierce, D. T.; Geiger, W. E. Electrochemical Kinetic Discrimination of the Single-Electron-Transfer Events of a Two-Electron-Transfer Reaction: Cyclic Voltammetry of the Reduction of the Bis(Hexamethylbenzene)Ruthenium Dication. *J. Am. Chem. Soc.* **1992**, *114* (15), 6063−6073.

(29) Evans, D. H. One-Electron and Two-Electron Transfers in Electrochemistry and Homogeneous Solution Reactions. *Chem. Rev.* **2008**, *108* (7), 2113−2144.

(30) Lexa, D.; Saveant, J. M. The Electrochemistry of Vitamin B12. *Acc. Chem. Res.* **1983**, *16* (7), 235−243.

(31) Liu, W.; Hempstead, M. R.; Nevin, W. A.; Melnik, M.; Lever, A. B. P.; Leznoff, C. C. Disproportionation, Electrochemistry, and Electronic Coupling Involving Mononuclear and Binuclear Cobalt Phthalocyanine Derivatives. *J. Chem. Soc., Dalton Trans.* **1987**, No. 11, 2511−2518.

(32) Bond, A. M.; Martin, R. L. Electrochemistry and Redox Behaviour of Transition Metal Dithiocarbamates. *Coord. Chem. Rev.* **1984**, *54*, 23−98.

(33) Avdeef, A.; Fackler, J. P.; Fischer, R. G. Structural Characterization of Tris(N,N-Di-n-Butyldithiocarbamato)Nickel(IV) Bromide. A Ni-S6 Complex with Unusual Chemical Properties. *J. Am. Chem. Soc.* **1970**, *92* (23), 6972−6974.

(34) Fackler, J. P.; Avdeef, A.; Fischer, R. G. Sulfur Chelates. XVI. Chemical Properties of Oxidized Nickel(II) Dithiocarbamates. X-Ray Crystal Structure of Tris(N,N-Dibutyldithiocarbamato)Nickel(IV)-Bromide, NiC27H54N3S6Br. *J. Am. Chem. Soc.* **1973**, *95* (3), 774−782.

(35) Chen, W.; Li, H.; Zhong, Z. J.; Zhang, K.; You, X. Z. Tris(N,N-Diethyldithiocarbamato-S,S')Nickel(IV) 1,1,2,3,3-Pentacyanopropenide. *Acta Crystallogr., Sect. C: Cryst. Struct. Commun.* **1996**, *52* (12), 3030−3033.

(36) Hogarth, G. Transition Metal Dithiocarbamates: 1978−2003. In *Progress in Inorganic Chemistry*; Karlin, K. D., Ed.; John Wiley & Sons, Inc., 2005; Vol. 53, pp 71−561.

DOI: 10.1021/acs.inorgchem.9b02430
Inorg. Chem. XXXX, XXX, XXX−XXX

(37) Fackler, J. P.; Coucouvanis, D. Sulfur Chelates. III. Metal Complexes of the 1,1-Dithiolato Anions S2CS2−, S2CNCN2−, and S2CC(CN)22−. *J. Am. Chem. Soc.* **1966**, *88* (17), 3913−3920.
(38) Coucouvanis, D.; Fackler, J. P. Square-Planar Sulfur Complexes. VI. Reactions of Bases with Xanthates, Dithiocarbamates, and Dithiolates of Nickel(II). *Inorg. Chem.* **1967**, *6* (11), 2047−2053.
(39) Stiefel, E. I.; Waters, J. H.; Billig, J. H. W. E.; Gray, H. B. The Myth of Nickel(III) and Nickel(IV) in Planar Complexes. *J. Am. Chem. Soc.* **1965**, *87* (13), 3016−3017.
(40) Kirk, M. L.; McNaughton, R. L.; Helton, M. E. The Electronic Structure and Spectroscopy of Metallo-Dithiolene Complexes. In *Dithiolene Chemistry: Synthesis, Properties, and Applications*; Stiefel, E. I., Ed.; Karlin, K. D., Series Ed.; Progress in Inorganic Chemistry; John Wiley & Sons, Ltd., 2004; Vol. *52*, pp 111−212.
(41) Williams, R.; Billig, E.; Waters, J. H.; Gray, H. B. The Toluenedithiolate and Maleonitriledithiolate Square-Matrix Systems. *J. Am. Chem. Soc.* **1966**, *88* (1), 43−50.
(42) Kobayashi, A.; Fujiwara, E.; Kobayashi, H. Single-Component Molecular Metals with Extended-TTF Dithiolate Ligands. *Chem. Rev.* **2004**, *104* (11), 5243−5264.
(43) Meucci, E. A.; Camasso, N. M.; Sanford, M. S. An Organometalllic NiIV Complex That Participates in Competing Transmetalation and C(Sp2)−O Bond-Forming Reductive Elimination Reactions. *Organometallics* **2017**, *36* (2), 247−250.
(44) Chong, E.; Kampf, J. W.; Ariafard, A.; Canty, A. J.; Sanford, M. S. Oxidatively Induced C−H Activation at High Valent Nickel. *J. Am. Chem. Soc.* **2017**, *139* (17), 6058−6061.
(45) Camasso, N. M.; Canty, A. J.; Ariafard, A.; Sanford, M. S. Experimental and Computational Studies of High-Valent Nickel and Palladium Complexes. *Organometallics* **2017**, *36* (22), 4382−4393.
(46) Bour, J. R.; Camasso, N. M.; Meucci, E. A.; Kampf, J. W.; Canty, A. J.; Sanford, M. S. Carbon-Carbon Bond-Forming Reductive Elimination from Isolated Nickel(III) Complexes. *J. Am. Chem. Soc.* **2016**, *138* (49), 16105−16111.
(47) Bour, J. R.; Camasso, N. M.; Sanford, M. S. Oxidation of Ni(II) to Ni(IV) with Aryl Electrophiles Enables Ni-Mediated Aryl-CF3 Coupling. *J. Am. Chem. Soc.* **2015**, *137* (25), 8034−8037.
(48) Camasso, N. M.; Sanford, M. S. Design, Synthesis, and Carbon-Heteroatom Coupling Reactions of Organometallic Nickel(IV) Complexes. *Science* **2015**, *347* (6227), 1218−20.
(49) Schultz, J. W.; Fuchigami, K.; Zheng, B.; Rath, N. P.; Mirica, L. M. Isolated Organometallic Nickel(III) and Nickel(IV) Complexes Relevant to Carbon-Carbon Bond Formation Reactions. *J. Am. Chem. Soc.* **2016**, *138* (39), 12928−12934.
(50) Zheng, B.; Tang, F.; Luo, J.; Schultz, J. W.; Rath, N. P.; Mirica, L. M. Organometallic Nickel(III) Complexes Relevant to Cross-Coupling and Carbon−Heteroatom Bond Formation Reactions. *J. Am. Chem. Soc.* **2014**, *136* (17), 6499−6504.
(51) Martinez, G. E.; Ocampo, C.; Park, Y. J.; Fout, A. R. Accessing Pincer Bis(Carbene) Ni(IV) Complexes from Ni(II) via Halogen and Halogen Surrogates. *J. Am. Chem. Soc.* **2016**, *138* (13), 4290−4293.
(52) Watson, M. B.; Rath, N. P.; Mirica, L. M. Oxidative C−C Bond Formation Reactivity of Organometallic Ni(II), Ni(III), and Ni(IV) Complexes. *J. Am. Chem. Soc.* **2017**, *139* (1), 35−38.
(53) Connelly, N. G.; Geiger, W. E. Chemical Redox Agents for Organometallic Chemistry. *Chem. Rev.* **1996**, *96* (2), 877−910.
(54) Saveant, J. M. *Elements of Molecular and Biomolecular Electrochemistry*; John Wiley & Sons, Inc., 2006.
(55) Nadjo, L.; Saveant, J. M. Linear Sweep Voltammetry: Kinetic Control by Charge Transfer and/or Secondary Chemical Reactions I. Formal Kinetics. *J. Electroanal. Chem.* **1973**, *48* (1), 113−145.
(56) Andrieux, C.; Nadjo, L.; Saveant, J. M. Electrodimerization VII. Electrode and Solution Electron Transfers in the Radical—Substrate Coupling Mechanism. Discriminative Criteria from the Other Mechanisms in Voltammetric Studies (Linear Sweep, Rotating Disc, Polarography). *J. Electroanal. Chem.* **1973**, *42* (2), 223−242.
(57) Nafady, A.; Costa, P. J.; Calhorda, M. J.; Geiger, W. E. Electrochemical Oxidation of CoCp(CO)2: Radical−Substrate Reaction of a 17 e-/18 e- Pair and Production of a Unique Dimer Radical. *J. Am. Chem. Soc.* **2006**, *128* (51), 16587−16599.
(58) Lam, K.; Geiger, W. E. Anodic Oxidation of Disulfides: Detection and Reactions of Disulfide Radical Cations. *J. Org. Chem.* **2013**, *78* (16), 8020−8027.
(59) Elgrishi, N.; Kurtz, D. A.; Dempsey, J. L. Reaction Parameters Influencing Cobalt Hydride Formation Kinetics: Implications for Benchmarking H2-Evolution Catalysts. *J. Am. Chem. Soc.* **2017**, *139* (1), 239−244.
(60) Lee, C.-M.; Chen, C.-H.; Ke, S.-C.; Lee, G.-H.; Liaw, W.-F. Mononuclear Nickel(III) and Nickel(II) Thiolate Complexes with Intramolecular S−H Proton Interacting with Both Sulfur and Nickel: Relevance to the [NiFe]/[NiFeSe] Hydrogenases. *J. Am. Chem. Soc.* **2004**, *126* (27), 8406−8412.
(61) De Castro, B.; Freire, C. EPR and Electrochemical Study of Nickel(III) Complexes of Bis(3,5-Dichlorosalicylaldehyde) o-Phenylenediimine. Evidence for Adduct Formation with Pyridines. *Inorg. Chem.* **1990**, *29* (25), 5113−5119.
(62) Vigee, G. S.; Watkins, C. L. Pyridine Adduct Complexes of Bis(N,N-Dithiocarbamate)Nickel(II). *J. Inorg. Nucl. Chem.* **1972**, *34* (12), 3936−3939.
(63) Nicholson, R. S.; Shain, I. Experimental Verification of an ECE Mechanism for the Reduction of *p* -Nitrosophenol, Using Stationary Electrode Polarography. *Anal. Chem.* **1965**, *37* (2), 190−195.
(64) Nicholson, R. S.; Shain, I. Theory of Stationary Electrode Polarography. *Anal. Chem.* **1964**, *36* (4), 706−723.
(65) Baucom, E. I.; Drago, R. S. Nickel(II) and Nickel(IV) Complexes of 2,6-Diacetylpyridine Dioxime. *J. Am. Chem. Soc.* **1971**, *93* (24), 6469−6475.
(66) Davis, D. G.; Boudreaux, E. A. Nickel(IV) Dimethylglyoxime. *J. Electroanal. Chem.* **1964**, *8*, 434−441.
(67) Zilbermann, I.; Maimon, E.; Cohen, H.; Meyerstein, D. Redox Chemistry of Nickel Complexes in Aqueous Solutions. *Chem. Rev.* **2005**, *105* (6), 2609−2625.
(68) Mandal, S.; Gould, E. S. Electron Transfer. 126. Reductions of Oxime-Bound Nickel(IV). *Inorg. Chem.* **1995**, *34* (15), 3993−3997.
(69) Li, T. C.; Spokoyny, A. M.; She, C.; Farha, O. K.; Mirkin, C. A.; Marks, T. J.; Hupp, J. T. Ni(III)/(IV) Bis(Dicarbollide) as a Fast, Noncorrosive Redox Shuttle for Dye-Sensitized Solar Cells. *J. Am. Chem. Soc.* **2010**, *132* (13), 4580−4582.
(70) Klein, H.-F.; Bickelhaupt, A.; Jung, T.; Cordier, G. Syntheses and Properties of the First Octahedral Diorganonickel(IV) Compounds. *Organometallics* **1994**, *13* (7), 2557−2559.
(71) Klein, H.-F.; Bickelhaupt, A.; Lemke, M.; Sun, H.; Brand, A.; Jung, T.; Röhr, C.; Flörke, U.; Haupt, H.-J. Trimethylphosphine Complexes of Diorganonickel(IV) Moieties. *Organometallics* **1997**, *16* (4), 668−676.
(72) Carnes, M.; Buccella, D.; Chen, J. Y.-C.; Ramirez, A. P.; Turro, N. J.; Nuckolls, C.; Steigerwald, M. A Stable Tetraalkyl Complex of Nickel(IV). *Angew. Chem., Int. Ed.* **2009**, *48* (2), 290−294.
(73) Dimitrov, V.; Linden, A. A Pseudotetrahedral, High-Oxidation-State Organonickel Compound: Synthesis and Structure of Bromotris(1-Norbornyl)Nickel(IV). *Angew. Chem., Int. Ed.* **2003**, *42* (23), 2631−2633.
(74) Mattson, B. M.; Heiman, J. R.; Pignolet, L. H. Oxidation of Tris(N,N-Disubstituted-Dithiocarbamato) Complexes of Ruthenium-(III). X-Ray Structure Determination of Bis(N,N-Diethyldithiocarbamato)-.Mu.-Tris(N,N-Diethyldithiocarbamato)-Diruthenium(III) Tetrafluoroborate, [Ru2(Et2dtc)5]BF4. *Inorg. Chem.* **1976**, *15* (3), 564−571.
(75) Hendrickson, A. R.; Martin, R. L.; Taylor, D. Synthesis and Properties of Dimeric Cobalt(Ii1) Dithiocarbamate Com- Plexes [Co2(R,Dtc),]+: X-Ray Structural Analysis of Pentakis-(Diethyldithiocarbamato)Dicobalt(Iii) Tetrafluoroborate. *J. Chem. Soc., Dalton Trans.* **1975**, 2182−2188.
(76) Bond, A. M.; Colton, R.; Ho, Y.; Moir, J. E.; Page, D. R.; Stott, R. Characterization of Pentakis(Dithiocarbamato)Dicobalt(III) Complexes, [Co2(RR'dtc)5]+, and Related Complexes in Dichloro-

DOI: 10.1021/acs.inorgchem.9b02430
Inorg. Chem. XXXX, XXX, XXX−XXX

methane Using Electrochemical and Cobalt-59 NMR Techniques. *Inorg. Chem.* **1985**, *24* (25), 4402−4407.
(77) Bond, A. M.; Hendrickson, A. R.; Martin, R. L.; Moir, J. E.; Page, D. R. Electrochemical Reduction and Oxidation of Cobalt(III) Dithiocarbamates. *Inorg. Chem.* **1983**, *22* (23), 3440−3446.
(78) Chant, R.; Hendrickson, A. R.; Martin, R. L.; Rohde, N. M. Tris(Dithiocarbamato) Complexes of Iron(II), Iron(III), and Iron-(IV). Electrochemical Study. *Inorg. Chem.* **1975**, *14* (8), 1894−1902.
(79) Emmenegger, F. P. A 1,10-Phenanthroline Adduct Complex of Bis(N,N-Diethyldithiocarbamato)Nickel(II). *Inorg. Chem.* **1989**, *28* (11), 2210−2214.
(80) Hollingsworth, N.; Roffey, A.; Islam, H.-U.; Mercy, M.; Roldan, A.; Bras, W.; Wolthers, M.; Catlow, C. R. A.; Sankar, G.; Hogarth, G.; et al. Active Nature of Primary Amines during Thermal Decomposition of Nickel Dithiocarbamates to Nickel Sulfide Nanoparticles. *Chem. Mater.* **2014**, *26* (21), 6281−6292.

DOI: 10.1021/acs.inorgchem.9b02430
Inorg. Chem. XXXX, XXX, XXX−XXX